GDE transmembrane ecto-enzymes : novel signaling functions through GPI-anchor cleavage

Veen, T.P.M. van

PINUS SYLVESTRIS

Chapter 3

Glycerophosphodiesterase GDE2 Promotes Neuroblastoma Differentiation through Glypican Release and is a Marker of Clinical Outcome

Cancer Cell 2016;30:548-562.

Elisa Matas-Rico[1], Michiel van Veen[1], Daniela Leyton-Puig[1], Jeroen van den Berg[1], Jan Koster[2], Katarzyna M. Kedziora[1], Bas Molenaar[1], Marjolein J.A. Weerts[1], Iris de Rink[3], René H. Medema[1], Ben N.G. Giepmans[1,5], Anastassis Perrakis[4], Kees Jalink[1], Rogier Versteeg[2], and Wouter H. Moolenaar[1]

[1] Division of Cell Biology, The Netherlands Cancer Institute, Amsterdam, Netherlands
[2] Department of Oncogenomics, Academic Medical Center, University of Amsterdam, Amsterdam, Netherlands
[3] Deep Sequencing Core Facility
[4] Division of Biochemistry, The Netherlands Cancer Institute, Amsterdam, Netherlands
[5] Present address: Department of Cell Biology, University Medical Center Groningen, Groningen, the Netherlands

Abstract

Neuroblastoma is a pediatric embryonal malignancy characterized by impaired neuronal differentiation. A better understanding of neuroblastoma differentiation is essential for developing new therapeutic approaches. GDE2 (encoded by *GDPD5*) is a six-transmembrane-domain glycerophosphodiesterase that promotes embryonic neurogenesis. We find that high *GDPD5* expression is strongly associated with favorable outcome in neuroblastoma. GDE2 induces differentiation of neuroblastoma cells, suppresses cell motility and opposes RhoA-driven neurite retraction. GDE2 alters the Rac-RhoA activity balance and the expression of multiple differentiation-associated genes. Mechanistically, GDE2 acts by cleaving (in *cis*) and releasing glycosylphosphatidylinositol-anchored glypican-6, a putative co-receptor. A single point mutation in the ectodomain abolishes GDE2 function. Our results reveal GDE2 as a cell-autonomous inducer of neuroblastoma differentiation with prognostic significance and potential therapeutic value.

Introduction

Neuroblastoma is a childhood cancer of the developing sympathetic nervous system, and the most common cancer in infancy. It develops from immature neuroblasts in the embryonic neural crest and is characterized by impaired neuronal differentiation [159-161]. It commonly originates in the adrenal gland, but can also develop in nerve tissues elsewhere in the body. Neuroblastoma is a highly heterogeneous disease. In some cases, the tumor undergoes spontaneous regression through mechanisms that remain poorly understood [162]. In many cases, however, neuroblastoma progresses into a high-risk metastatic disease with very poor prognosis. Remarkably, high-risk neuroblastoma is characterized by relatively few recurrent somatic mutations [163, 164]. The paucity of oncogenic mutations, along with an incomplete understanding of neuroblastoma differentiation and regression, hampers the development of new targeted therapies.

In general, overall survival of neuroblastoma patients is largely dependent on the degree of neuronal differentiation and, furthermore, inversely correlated with a motile phenotype [160, 165]. Consistent with this, some high-risk neuroblastomas are associated with mutations in Rac-Rho pathway genes that normally regulate F-actin-based neurite outgrowth and remodeling, as well as tumor cell motility, invasion and metastasis [163]. Unfortunately, treatment options are very limited for high-risk neuroblastoma. One strategy involves differentiation therapy using *cis*-retinoic acid, but this has led to disappointing results [166-168]. Thus, there remains an urgent need to identify new therapeutic targets and develop differentiation-inducing protocols [169]. A better understanding of neuroblastoma differentiation at the molecular level is therefore imperative.

In this study we focus on GDE2 (or GDPD5), a transmembrane ecto-phosphodiesterase that promotes embryonic neurogenesis [108]. GDE2/GDPD5, along with GDE3/GDPD2 and GDE6/GDPD4, belongs to a subfamily of glycerophosphodiester phosphodiesterases (GDEs or GDPDs) characterized by six transmembrane domains and a large catalytic ectodomain [96, 97] (Figure 1A,B). GDE2 promotes the differentiation of postmitotic motor neurons in vivo by inhibiting Notch signaling in adjacent neural progenitors [109]. GDE3 has been implicated in osteoblast differentiation [99, 115], while the function of GDE6 is unknown. Mechanistically, GDE2 acts by cleaving the gycosylphosphatidylinositol (GPI) anchor of RECK, a Notch ligand regulator, leading to RECK release from the cell surface and subsequent induction of differentiation in contacting neuronal cells [110]. Thus, GDE2 promotes neurogenesis in a non-cell-autonomous manner, requiring cell-cell contact, at least in the developing spinal cord.

In view of these findings, we set out to examine a possible role of GDE2 in regulating neuroblastoma differentiation.

Results

GDPD5 Expression Levels Strongly Correlate with Clinical Outcome in Neuroblastoma

We examined how *GDPD5* expression relates to overall survival in neuroblastoma, using mRNA expression data of primary tumor samples from three independent patient cohorts (AMC, Obertheuer and RPM datasets; n=871 patients). *GDPD5* maps to chromosome 11q13, a region often showing loss of heterozygosity in neuroblastoma [159], Kaplan-Meier analysis revealed that high *GDPD5* expression is strongly associated with favorable clinical outcome, while low *GDPD5* expression correlates with poor outcome in all three patient cohorts (Figure 1C). This marks *GDPD5* as a potential tumor suppressor, but no mutations or deletions were detected in tumor samples analyzed by whole genome sequencing [163]. Furthermore, *GDPD5* expression in patients with an 11q deletion was similar to those with a normal chromosome 11, while there was no significant association with *MYCN* amplification (p=0.08) or *ALK* mutation status (p=0.66, Fisher's Exact test; data not shown),

GDE2 promotes neurogenesis through loss of functional RECK [110]; however, we found no significant correlation between *RECK* expression and patient survival (data not shown). Of note, GDE2 family members GDE3 and GDE6 (encoded by *GDPD2* and *GDPD4*, respectively; Figure 1A) were not detectably expressed at the mRNA level in the tumors analyzed, and therefore appear not to have clinical significance in neuroblastoma. These results define high *GDPD5* expression as a favorable prognostic marker in neuroblastoma. We went on to examine how GDE2 affects neuroblastoma cell behavior and to explore its signaling functions and pertinent catalytic activity.

GDE2 Promotes Differentiation of Neuroblastoma Cells in an Autonomous Manner

We used established models of neuroblastoma differentiation, including SH-SY5Y, IMR-32, Neuro-2A and N1E-115 cells; in the latter cells, Rho/Rac signaling and neurite remodeling pathways have been extensively studied. Overexpression of GDE2 in N1E-115 or Neuro-2A cells resulted in prominent cell spreading and neurite outgrowth (Figure 2A-C, Figure S1A). Similarly, expression of doxycycline-inducible GDE2 in either SH-SY5Y or IMR-32 cells led to GDE2 overexpression concomitant with increased neurite outgrowth after doxycycline addition (Figure 2D,E). GDE2-induced neurite outgrowth was accompanied by upregulation of various established neural differentiation genes, including *NEUROD1*, *SNAP25*, *ENO2, TUBB3* and *MAP2* (Figure 2F).

During embryonic development, GDE2 promotes neurogenesis in non-cell-autonomous manner involving contact-dependent Notch signaling [109]. In neuroblastoma cells, however, GDE2-induced cell spreading and neurite formation was observed in both isolated and contacting cells (Figure S1B). Furthermore, conditioned medium from GDE2-overexpressing cells did not affect the morphology of parental cells (results not shown), arguing against the

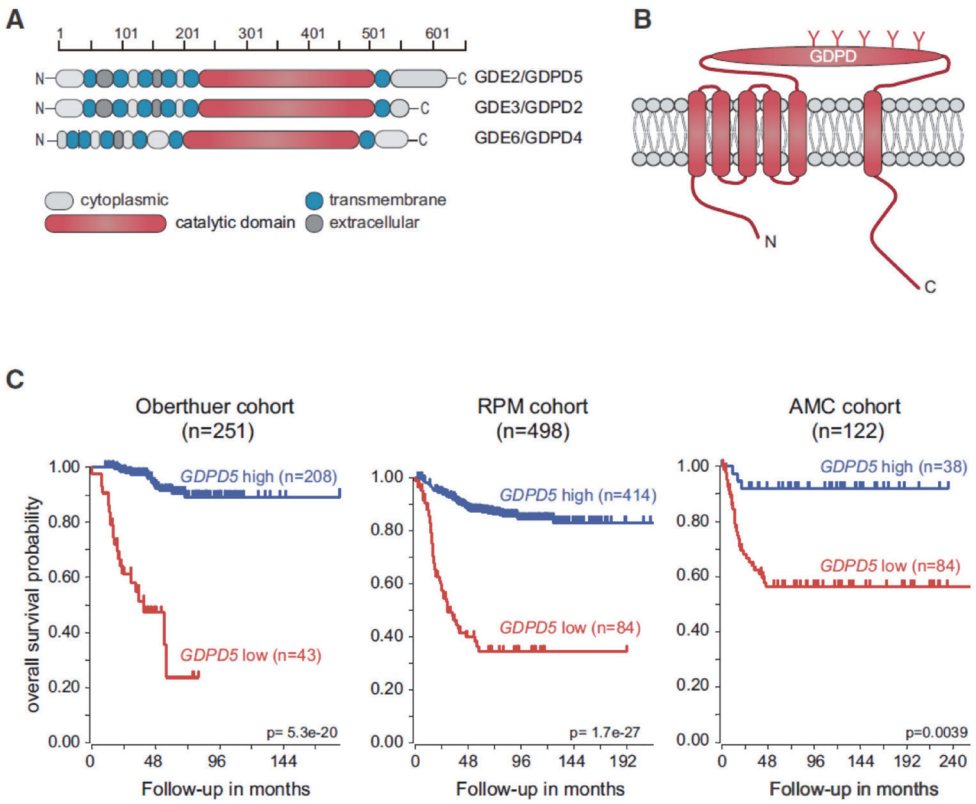

Figure 1. GDE2: its Family Members and Prognostic Significance in Neuroblastoma
(A) GDE2 (or GDPD5) and its close relatives GDE3 (GDPD2) and GDE6 (GDPD4) contain six transmembrane domains and a large catalytic ectodomain, as illustrated. **(B)** Schematic representation of GDE2, with five potential N-glycosylation sites indicated. **(C)** Kaplan-Meier analysis of overall survival in three independent neuroblastoma patient cohorts, as indicated: Oberthuer (n=251; ArrayExpress: E-TABM-38), Neuroblastoma RPM/SEQC (n=498; GEO: GSE62564) and AMC/Versteeg (n=122; GEO: GSE16476 88/122). The graphs depict the p values corrected for the multiple testing (Bonferroni correction) of cut-off levels for *GDPD5*. Family members *GDPD2* and *GDPD4* were not detectably expressed in the tumor samples analyzed.

involvement of a diffusible factor produced by GDE2. It thus appears that GDE2 promotes neuroblastoma differentiation in a cell-autonomous manner, not requiring cell-cell contact.

Various human neuroblastoma cells, including SH-SY5Y, are responsive to retinoic acid (RA), a known inducer of neuronal differentiation that is used as a therapeutic in the clinic [166, 169, 170]. RA upregulates GDE2 expression in the ventricular zone [108] and in Neuro-2A cells [107], but it did not in SH-SY5Y cells (Figure S1C). Upon forced overexpression

in SH-SY5Y cells, GDE2 enhanced the neurite-inducing effect of RA (2 μM) (Figure S1D), strongly suggesting that GDE2 and RA act cooperatively to induce differentiation.

GDE2-overexpresssing SH-SY5Y and IMR-32 cells adhered markedly stronger to extracellular matrix molecules (laminin, fibronectin, collagen) than did the parental cells (Figure 2G). Cell-matrix adhesion is a major determinant of cell motility, and a motile phenotype is associated with increased incidence of metastases and poor prognosis in neuroblastoma [165]. By monitoring the random motility of SH-SY5Y and IMR-32 cells, we established that GDE2 overexpression renders the cells less motile than the wild-type cells (Figure 2H).

When expressed at relatively low levels, GDE2 was detected both at the plasma membrane and in intracellular compartments as revealed by confocal and super-resolution microscopy (Figure S1E,F). Plasma membrane GDE2 localized to distinct microdomains, possibly representing lipid rafts, and was particularly enriched at the tips of neurite-like extensions (Figure S1F). Intracellularly, a relatively large subset of GDE2-containing vesicles was positive for established markers of recycling endosomes, notably Rab11 and the transferrin receptor (TfR) [171, 172] (Figure S1G,H). This suggests that internalized GDE2 follows a Rab11-driven recycling route as a way of regulation. We further note that, once internalized, GDE2 has its catalytic ectodomain exposed to the vesicle lumen and hence cannot act on cytosolic substrates.

⟶ **Figure 2. GDE2 Induces Neuroblastoma Cell Differentiation and Suppresses Cell Motility (A,B)**

Images of N1E-115 cells expressing GDE2-mCh or GDE2-GFP. Note flattened morphology and neurite outgrowth in GDE2-ovexpressing cells (A, black arrows), when compared to non-transfected cells. Bar, 10 μm. In (B), cells were stained with phalloidin to visualize F-actin. Cells transfected with empty vector were used as control. GDE2-GFP in green, F-actin in red. Bar, 10 μm. **(C)** Quantitative analysis of distinct morphologies of GDE2-overexpressing versus empty vector-expressing cells. (Left) Percentage of cells with a round or flattened morphology (assayed in the presence of serum). (Middle) Neurite induction; (Right) Neurite length (three independent experiments; n>300 cells; error bars, mean ± SEM) **** p value < 0.0001 of Fisher's (left, middle) and unpaired t tests (right). **(D)** SH-SY5Y and IMR-32 cells containing doxycyclin (Dox)-inducible GDE2 show longer neurites after Dox (1 μM) addition (bar, 100 μm). Immunoblots (using anti-GDE2 antibody) show Dox-induced GDE2 expression over a 3-72 hr time period. **(E)** Quantification of Dox-induced neurite outgrowth (n = 250 cells; mean ± SEM). **(F)** Dox-induced GDE2 overexpression promotes induction of neural differentiation marker genes *NEUROD1*, *SNAP25*, *ENO2*, *TUBB3* and *MAP2*, but not *NPY* and *GAP43*, as determined by qPCR in SH-SY5Y cells. Error bars represent SEM of triplicate measurements. **(G)** Dox-induced GDE2 overexpression promotes cell-matrix adhesion. At 1 hr after plating, adherent SH-SY5Y and IMR-32 cells were fixed and stained with Crystal Violet for quantification. Error bar represents SD of two independent experiments. **(H)** Random cell motility of individual SH-SY5Y and IMR-32 cells expressing inducible GDE2-mCh (red) or empty vector (black), plated on fibronectin. Tracks were generated from time-lapse movies (12 hr, 10-min. intervals). Graphs show mean migration distances of control versus GDE2-mCh-expressing SH0SY5Y and IMR-32 cells. In panels E-H, * p value < 0.05; ** p value <0.01 *** p value <0.001 **** p value <0.0001 of unpaired t-test. See also Figure S1.

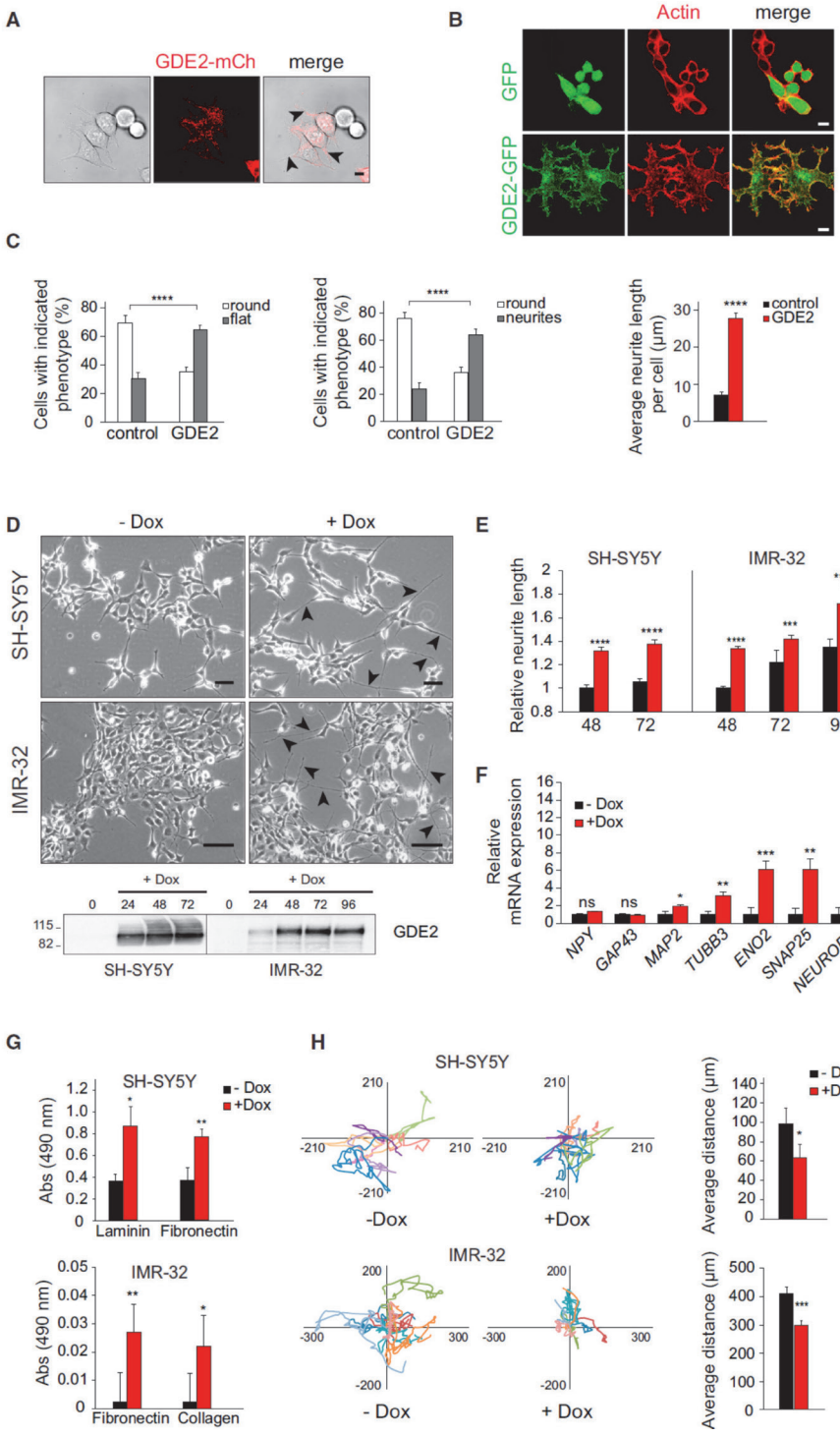
A
GDE2-mCh
merge
B
Actin
merge
GFP
GDE2-GFP
C
Cells with indicated phenotype (%)
round
flat
control
GDE2
round
neurites
Average neurite length per cell (µm)
control
GDE2
D
- Dox
+ Dox
SH-SY5Y
IMR-32
+ Dox
0 24 48 72
0 24 48 72 96
115
82
GDE2
SH-SY5Y
IMR-32
E
SH-SY5Y
IMR-32
- Dox
+Dox
Relative neurite length
48 72 48 72 96 [hr]
F
Relative mRNA expression
- Dox
+Dox
ns
NPY
GAP43
MAP2
TUBB3
ENO2
SNAP25
NEUROD1
G
SH-SY5Y
Abs (490 nm)
- Dox
+Dox
Laminin
Fibronectin
IMR-32
Fibronectin
Collagen
H
SH-SY5Y
-Dox
+Dox
IMR-32
- Dox
+ Dox
Average distance (µm)
- Dox
+Dox

GDE2 Opposes RhoA-Mediated Neurite Retraction and Activates Rac

Rho GTPases, particularly RhoA, Rac and Cdc42, are key regulators of F-actin-driven processes, including neuronal differentiation, cell adhesion, motility and invasion [173-177]. One hallmark of developing neurites is their susceptibility to acute retraction by RhoA-activating agonists such as lysophosphatidic acid (LPA), a lipid mediator acting on specific G protein-coupled receptors. As such, LPA antagonizes the phenotypic differentiation of neuroblastoma and neural/stem progenitor cells [178-182]. Strikingly, GDE2-overexpressing N1E-115 cells were unable to retract their developing neurites and round up in response to LPA, whereas the parental cells responded vigorously (Figure 3A,B; Figure S2; Movie S1 and S2). The apparent loss of LPA/GPCR responsiveness upon GDE2 overexpression is reminiscent of an activated Tiam1-Rac phenotype, where Rac hyperactivation is sufficient to inhibit LPA/RhoA-induced cytoskeletal contraction [183, 184]. GDE2-overexpressing N1E-115 or SH-SY5Y cells indeed showed a marked increase in basal Rac activity, which was insensitive to LPA stimulation (Figure 3C). Furthermore, we confirmed that expression of hyperactive Rac(L61A) induced prominent neuroblastoma cell spreading and conferred complete resistance to cytoskeletal contraction by LPA (results not shown).

Active Rac is known to oppose RhoA at multiple levels [175, 183-186]. We monitored LPA-induced RhoA activation in real-time using a RhoA-specific FRET-based biosensor, as described [187]. In parental N1E-115 cells, LPA evoked an immediate increase in RhoA activity that gradually levelled off to a sustained elevated level (Figure 3D). Upon GDE2 overexpression, however, the magnitude of LPA-induced RhoA activation was about 3-fold reduced (Figure 3D). Decreased RhoA activation was also observed in SH-SY5Y cells (Figure

⟶ **Figure 3. GDE2 Opposes RhoA-driven Neurite Retraction by LPA and Activates Rac** **(A)** Serum-starved N1E-115 cells expressing GDE2-mCh were stimulated with LPA (1 μM) for the indicated times. GDE2-mCh-expressing cells are indicated by black arrows, non-transfected cells by white arrows. Bar, 10 μm. **(B)** Quantification of LPA-induced cell rounding over time in control and GDE2- overexpressing cells (n= 200 cells; mean ± SEM). * p value < 0.05; *** p value < 0.001 of unpaired t-test. **(C)** Rac activity was measured in cells expressing empty vector (pcDNA3) or GDE2-GFP. Active GTP-bound Rac was assessed by pull-down assays and compared to total Rac levels in lysates of the same transfectants. (Left) Effect of LPA stimulation on Rac-GTP levels. (Middle) Densitometry analysis of Rac-GTP versus total Rac levels in the presence or absence of LPA (mean ± SEM of three independent experiments). * p value < 0.05 of unpaired t-test. (Right) Western blot showing Rac activity in SH-SY5Y cells as a function of GDE2 expression and LPA stimulation. **(D)** (Left) Activation of RhoA in N1E-115 cells expressing either GDE2-mCherry (red trace) or mCherry-CAAX (black trace) was monitored by a FRET-based biosensor. An increase in YFP/CFP ratio indicates increased RhoA activity (see Experimental Procedures). (Middle) Maximum RhoA activation by LPA (n= 9, mean ± SEM). ** p value < 0.01 of Wilcoxon test. (Right) Western blot of RhoA-GTP levels in Dox-induced SH-SY5Y cells. **(E)** Confocal images of N1E-115 cells transfected with Myc-RhoA(V14A) or co-transfected with GDE2-mCh and stained for Myc. GDE2 in red, RhoA(V14A) in green. Bar graph shows quantitation of morphology of RhoA(V14A)-expressing versus RhoA(V14A)/GDE2 co-expressing cells (n=300 cells, mean ± SEM); * p value < 0.05 of unpaired t-test. Bar 10 μm. See also Figure S2 and Movie S1 and S2.

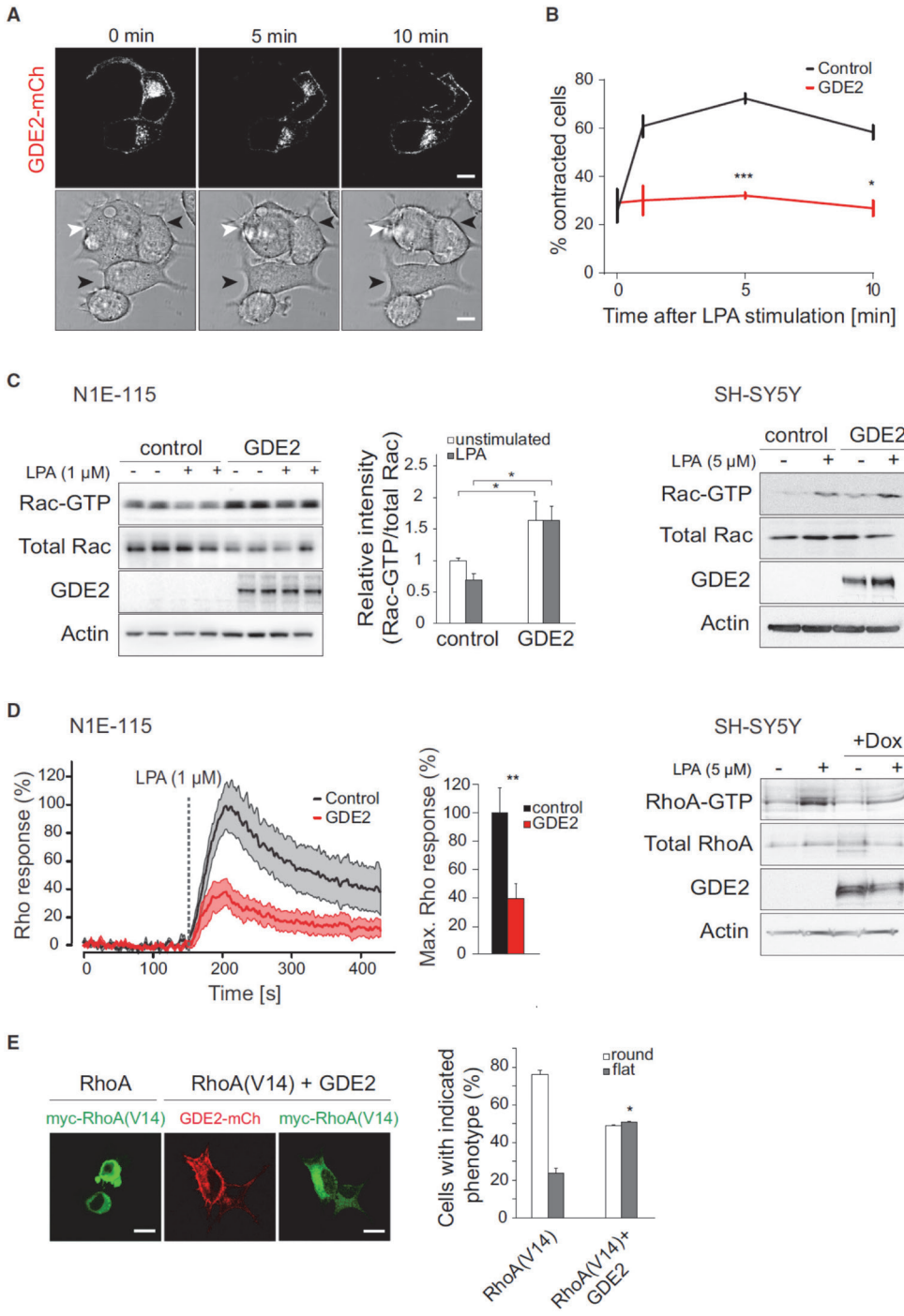
A
0 min
5 min
10 min
GDE2-mCh
B
% contracted cells
Control
GDE2
***
*
Time after LPA stimulation [min]
C
N1E-115
control
GDE2
LPA (1 µM)
Rac-GTP
Total Rac
GDE2
Actin
Relative intensity (Rac-GTP/total Rac)
unstimulated
LPA
control
GDE2
SH-SY5Y
LPA (5 µM)
D
N1E-115
LPA (1 µM)
Rho response (%)
Time [s]
Max. Rho response (%)
SH-SY5Y
+Dox
RhoA-GTP
Total RhoA
E
RhoA
RhoA(V14) + GDE2
myc-RhoA(V14)
GDE2-mCh
Cells with indicated phenotype (%)
round
flat
RhoA(V14)
RhoA(V14)+ GDE2

3D). Furthermore, overexpressed GDE2 opposed constitutively active RhoA(V14A) in promoting cell contraction, again consistent with an activated Rac phenotype (Figure 3E). From these results, along with previous findings on Rac-RhoA antagonism, we conclude that high GDE2 expression prevents neurite retraction by activating Rac and opposes RhoA action both at the level of RhoA-GTP accumulation and more downstream.

GDE2 Depletion Reverses the GDE2 Overexpression Phenotype and Uncovers GDE2-Regulated Gene Expression

Since low *GDPD5* expression correlates with poor clinical outcome, we examined how GDE2 depletion affects neuroblastoma phenotype through lentiviral shRNA transduction. To this end, we used Shep2 cells since these cells show relatively high *GDPD5* expression among 24 human neuroblastoma cell lines analyzed (Figure 4A; Figure S3). Using two (out of five) independent shRNAs, we achieved efficient GDE2 knockdown (Figure 4B). When compared to shControl cells, GDE2-depleted Shep2 cells were less well spread and

⟶ **Figure 4. GDE2 Depletion Reverses the GDE2 Overexpression Phenotype and Uncovers GDE2-Regulated Gene Expression**

(A) Immunoblot of GDE2 expression in the indicated cell lines, using anti-GDE2 antibody. See Figure S3 for *GDPD5* mRNA expression analysis. **(B)** (Left) *GDPD5* expression (relative to *GAPDH*) in control and GDE2-depleted Shep2 cells stably expressing shRNAs against GDE2. Maximal GDE2 knockdown was obtained with hairpins #4 and #5. Error bars, mean ± SEM; ** p value < 0.01; *** p value < 0.001 of unpaired t-test. (Right) Immunoblot analysis of GDE2 protein expression using five different hairpins, as indicated. Actin was used as loading control. **(C)** Rac-GTP levels in control and GDE2-depleted Shep2 cells (using hairpin #4). **(D)** Cell morphology and cytoskeletal organization (phalloidin and vinculin staining) in control and GDE2-depleted Shep2 cells Expression of RNAi-resistant GDE2 rescues the phenotype, as indicated. Black bar, 100 μm; white bar, 10 μm. **(E)** Immunoblot showing GDE2 expression in control, GDE2-depleted and "GDE2-rescued" Shep2 cells (transfected with RNAi-resistant GDE2). **(F)** Quantification of focal adhesion area in control, GDE2-depleted and GDE2-rescued Shep2 cells using Image J software (n=20 cells; mean ± SEM); **** p value < 0.0001 of one way ANOVA. **(G)** Cell-matrix adhesion of control, GDE2-depleted and rescued Shep2 cells. Cells were plated on fibronectin or collagen. At 30 min after plating, adherent cells were fixed and stained with Crystal Violet for quantification. Graph represents the mean ± SEM of two independent experiments; ** p value < 0.01; *** p value < 0.001 of unpaired t-test. **(H)** Analysis of random cell motility. (Left) Traces from individual cells are shown (control, GDE2 depleted and GDE2-rescued cells, as indicated). Tracks were generating from time-lapse movies. Images were captured every 10 min. for 12 hr. (Right) Quantification of mean migration distances (n≥ 60 cells, mean ± SEM); ** p value < 0.01; **** p value <0.0001 of unpaired t-test. **(I)** (Left) Heatmap showing differentially expressed genes upon GDE2 silencing in Shep2 cells as determined by whole-genome RNA-seq (cut-off: ^{2}log-fold change >1.5; p value < 0.001). Experiments were performed in duplicate, as indicated. For the complete list of genes with gene ontology (GO) annotations, see Table S1. (Right) Bar graph shows the GO terms that are significantly enriched among the differentially expressed genes. Transmembrane receptor signaling includes pathways mediated by G protein-coupled receptors, receptor protein tyrosine kinases, TGF-β, Wnt and Hedgehog. See also Table S1.

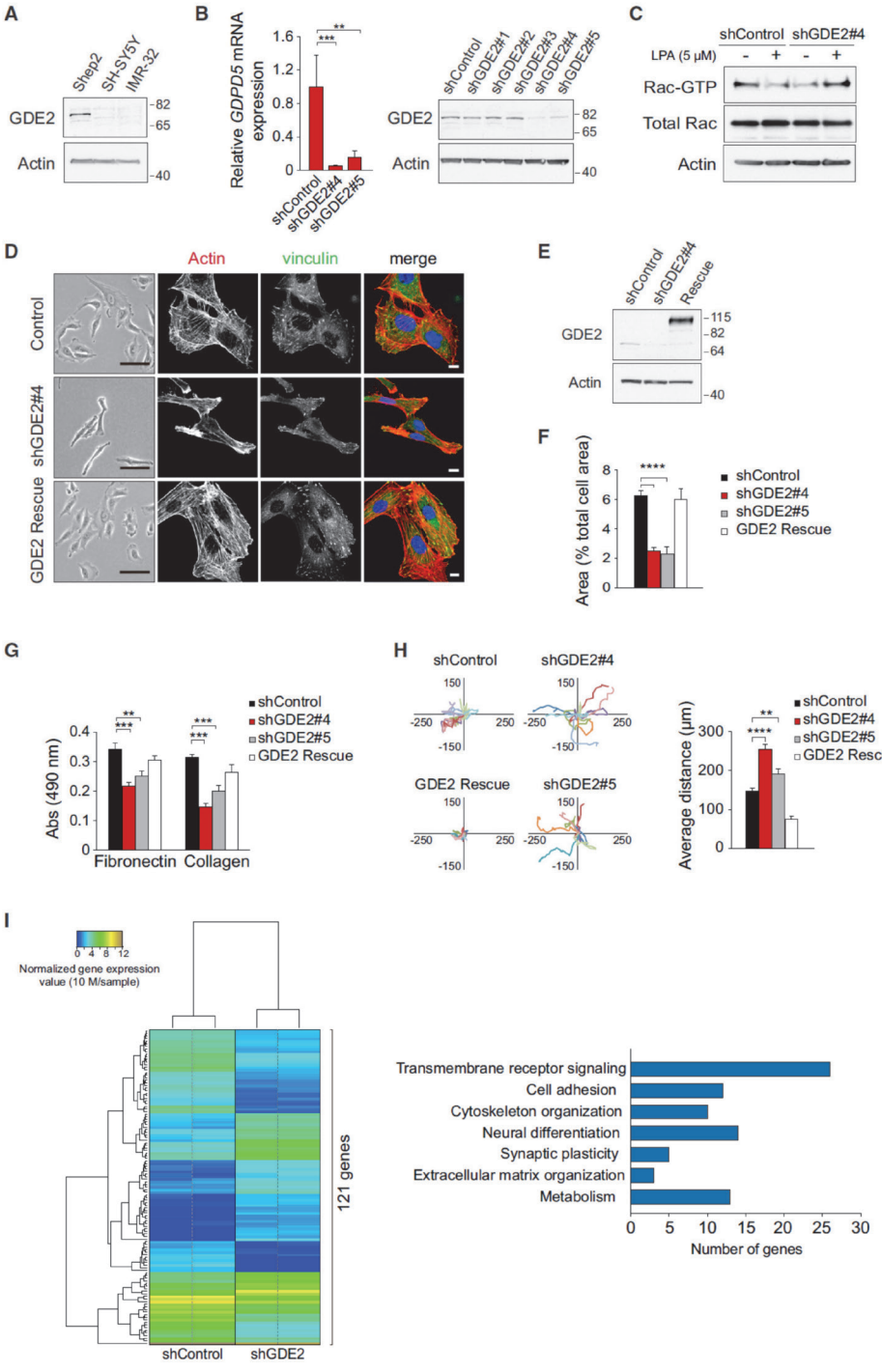
A
Shep2
SH-SY5Y
IMR-32
GDE2
Actin
82
65
40
B
Relative GDPD5 mRNA expression
1.6
1.2
0.8
0.4
0
**
***
shControl
shGDE2#4
shGDE2#5
shControl
shGDE2#1
shGDE2#2
shGDE2#3
shGDE2#4
shGDE2#5
GDE2
Actin
82
65
40
C
shControl
shGDE2#4
LPA (5 µM)
- + - +
Rac-GTP
Total Rac
Actin
D
Actin
vinculin
merge
Control
shGDE2#4
GDE2 Rescue
E
shControl
shGDE2#4
Rescue
GDE2
Actin
115
82
64
40
F
Area (% total cell area)
8
6
4
2
0
****
shControl
shGDE2#4
shGDE2#5
GDE2 Rescue
G
Abs (490 nm)
0.4
0.3
0.2
0.1
0
**
***
***
***
shControl
shGDE2#4
shGDE2#5
GDE2 Rescue
Fibronectin
Collagen
H
shControl
shGDE2#4
GDE2 Rescue
shGDE2#5
150
-250
250
-150
Average distance (µm)
300
200
100
0
**
****
shControl
shGDE2#4
shGDE2#5
GDE2 Rescue
I
0 4 8 12
Normalized gene expression value (10 M/sample)
121 genes
shControl
shGDE2
Transmembrane receptor signaling
Cell adhesion
Cytoskeleton organization
Neural differentiation
Synaptic plasticity
Extracellular matrix organization
Metabolism
0
5
10
15
20
25
30
Number of genes

smaller in size, and showed a reduction in basal Rac1 activity, which was now sensitive to LPA stimulation (Figure 4C). This was accompanied by marked cytoskeletal reorganization, less focal adhesions and reduced cell-matrix adhesion (Figure 4D-G). Moreover, GDE2 knockdown cells migrated faster and over longer distances than did shControl cells (Figure 4H). Shep2 cells were poorly responsive to LPA; upon GDE2 depletion, however, they showed more pronounced cytoskeletal contraction induced by LPA (results not shown). The knockdown phenotypes could be rescued by expression of RNAi-resistant GDE2, indicating that the observed effects are specific for GDE2 depletion (Figure 4D-H). Thus, GDE2 knockdown evokes phenotypic changes opposite to those induced by GDE2 overexpression.

Having shown that GDE2 activates Rac1 and opposes RhoA, we next examined how GDE2 may dictate neuroblastoma phenotype at the gene expression level. We analyzed differential gene expression in GDE2 knockdown versus shControl Shep2 cells using genome-wide RNA sequencing (RNA-seq). In duplicate experiments, RNA-seq-based analysis revealed 121 differentially expressed genes (^{2}log-fold change >1.5; p values <0.001) (Figure 4I; Table S1). The list of differentially expressed genes was markedly enriched (18%; 22/121) in those involved in neuronal differentiation, such a *RELN*, *NTM*, *ROBO4*, *RNF112, PLPPR4*, *KIRREL3*, and various genes (15%; 18/121) that regulate cell adhesion (*LAMA4, COL6A3, COL13A1, FN1, ITGA10, ITGA11*) and extracellular matrix organization (Table S1; Figure 4I). It is also noteworthy that some 20% (26/121) of the GDE2-regulated genes encodes proteins involved in transmembrane receptor activity, including signaling by receptor tyrosine kinases (*EPHB6, PDGFRA, TIE1, ERBB4*), GPCRs, Wnt, Hedgehog and TGF-β receptors, several of which play a role in neurodevelopment (Table S1). These data suggest a scenario where a unique set of differentiation regulatory genes, along with Rac hyperactivation, dictates the observed GDE2 phenotypes and may help explain the marked correlation between *GDPD5* expression and patient survival.

GDE2 Biochemical Activity: Release of GPI-Anchored Glypican-6

What is the relevant catalytic activity of GDE2 and how does it relate to the observed differentiated phenotype? Immunoprecipitated GDE2 hydrolyzes glycerophosphocholine into glycerol 3-phosphate [100], but this reaction has no signaling relevance. We examined GDE2 enzymatic activity using cell-based assays and mutational analysis. Prompted by the discovery that chicken GDE2 induces the release of GPI-anchored RECK from HEK293 cells [110], we measured GDE2 activity towards selected GPI-anchored proteins, including RECK and glypicans (GPCs). Glypicans are a family of six heparan sulfate proteoglycans that function as co-receptors or ligands to regulate diverse signaling pathways, either positively or negatively, particularly those involved in morphogenesis and neurodevelopment [188-190]. We co-expressed GDE2 and its candidate substrates, confirmed their proper expression at the plasma membrane (Figure S4A-C and data not shown), and assayed cell lysates

and the medium for substrate release by immunoblotting, essentially as described [110].

We confirmed that chicken GDE2 promotes the release of RECK, as did exogenous PI-PLC (Figure 5A). Unexpectedly, however, our efforts to detect RECK release by human GDE2 were unsuccessful (Figure 5A), suggesting that GDE2 substrate preferences may vary among vertebrates. We then examined the GPI-anchored glypicans as potential substrates. Human GDE2 induced the release of GPC3 and GPC6, but not that of GPC1, 2, 4 and 5 (Fig. S4D; Figure 5C). This indicates that GDE2 shows selectivity towards glypican family members, likely due to structural differences in the respective heparan sulfate chains and/or the GPI-anchor core.

GPC6 is widely expressed among neuroblastoma cell lines (Figure S4E), while GPC3 expression is more variable (Figure S4F). SH-SY5Y and N1E-115 cells express GPC6 but not GPC3 (Figure S4E,F,G and Figure 7A below). We therefore focused our subsequent experiments on GPC6. As one would predict, when co-expressed in N1E-115 cells, GDE2 and GPC6 co-localized in part to the same membrane microdomains (Figure S4B,C).

Mutating His233 Abolishes GDE2 Function

Uncertainty still exists as to the active site of GDE2. Residue His275 was reported to be critical for GDE2-induced neurogenesis [108]. Another potential catalytic residue is His233, located in a conserved GHRG motif [97] (Figure 5B). As shown in Figure 5C, mutants GDE2(H233A) and GDE2(H233A/275A) failed to induce the release of GPC6, whereas the H275A mutation reduced GDE2 activity only partially. This result defines His233 as key catalytic residue.

Previous in vivo studies suggested that GDE2 activity is enhanced after reduction of a putative disulfide bond (Cys25-Cys576) linking the N- and C-terminal tails [118] (Figure 5B), but the catalytic activity of relevant Cys mutants was not examined. In our glypican release assay, the supposedly hyperactive mutant GDE2(C25S), lacking the putative disulfide bond, showed the same catalytic activity as wild-type GDE2 (Figure 5D). This argues against a critical role for Cys25-Cys576 disulfide bonding/reduction in regulating GDE2 activity under the present assay conditions. Finally, to establish if GDE2 acts in *cis* (same cell) or/and in *trans* (adjacent cell), we mixed GDE2-expressing cells (lacking GPC6) with GPC6-expressing cells (lacking GDE2) and measured GPC6 release. GDE2-expressing cells were incapable of promoting GPC6 release from adjacent cells (Figure 5E). It thus appears that GDE2 acts in *cis*, consistent with GDE2 promoting differentiation in a cell-autonomous manner, not requiring intercellullar contacts.

When expressed in N1E-115 cells, catalytically dead GDE2(H233A) failed to promote cell spreading and neurite formation. GDE2(H275A) induced an intermediate phenotype, while the C25S mutation had no effect (Figure 6A-C), consistent with the above biochemical data. In addition, GDE2(H233A)-overexpressing cells showed a normal contractile response to LPA (results not shown). Thus, GDE2 catalytic activity is necessary and sufficient to induce neuroblastoma cell differentiation and to inhibit agonist-induced neurite retraction.

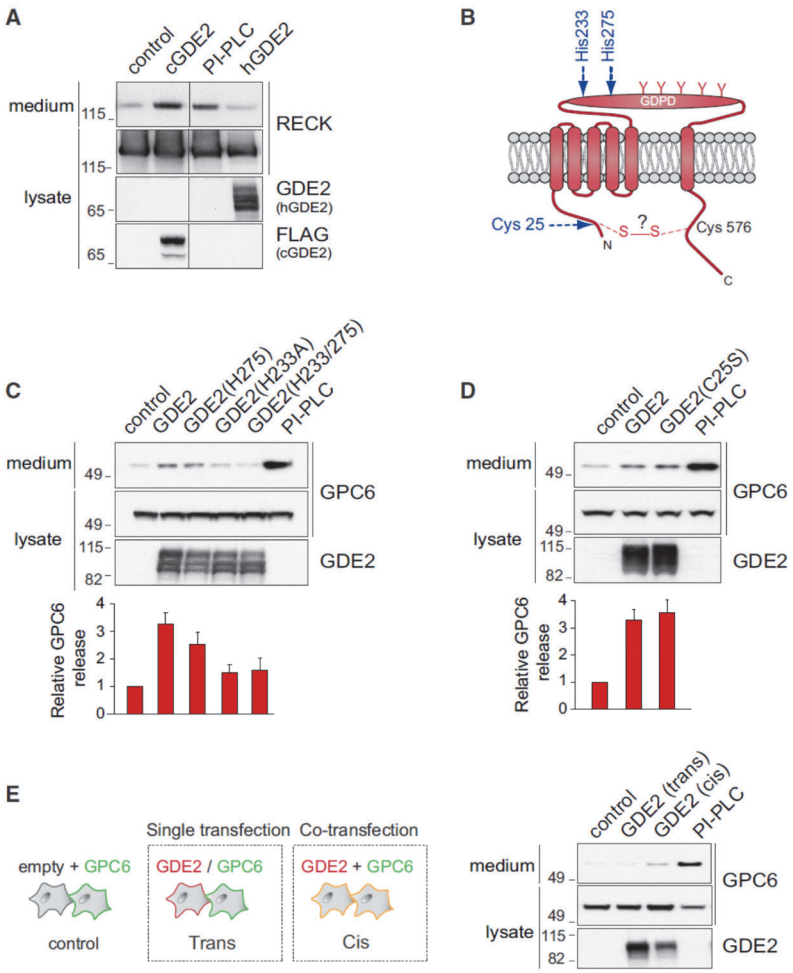

Figure 5. GDE2 Selectively Cleaves Glypican-6: Residue His233 is Essential for Activity

(A) HEK293 cells were co-transfected with RECK and either human GDE2-HA (hGDE2) or chicken GDE2-FLAG (cGDE2). Expression levels were assessed by immunoblotting in cell lysates and conditioned medium. PI-PLC was used as positive control in all experiments. **(B)** Schematic illustration of mutations made in GDE2. See text for details. **(C)** HEK293 cells were cotransfected with GPC6-HA and GDE2-mCh or the indicated mutants (GDE2(H27A), GDE2(H233A), GDE2(H233A/H275A)). The bar graph shows quantification of GPC6 released into the medium, as quantified using Image J software and expressed as GPC6 release relative to that in control cells. Error bars represent mean ± SEM of three independent experiments. **(D)** HEK293 cells transfected with GPC6-HA together with either GDE2-mCh or mutant GDE2(C25S)-mCh. Quantification of GPC6 release (bar graph) as in (C). **(E)** (Left) Scheme of the assay in HEK293 cells. GPC6-HA and GDE2-mCh co-transfected HEK293 cells or transfected with either GPC6-HA or GDE2-mCh were mixed and plated in PEI-coated plates. (Right) After 24 hr incubation in serum-free medium, GPC6 in the medium and cell lysates was analyzed by Western blotting. See also Figure S4.

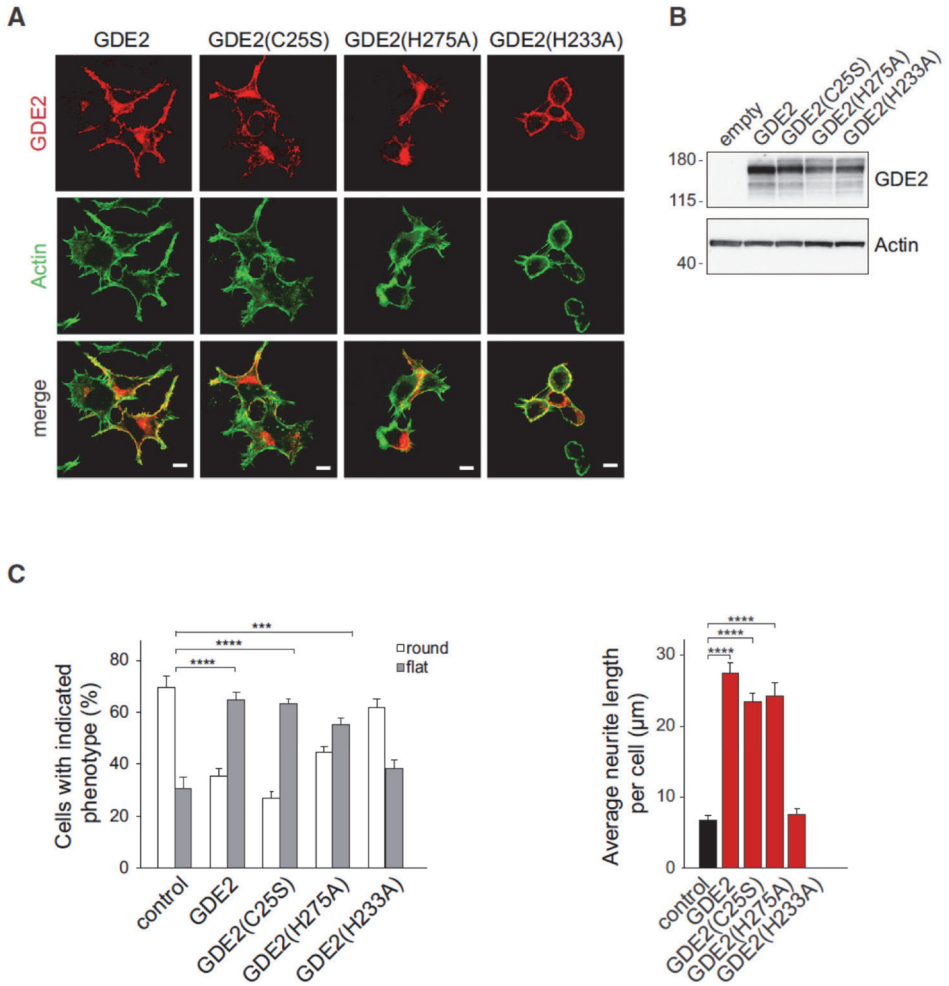

Figure 6. Mutating His233 Abolishes GDE2 Biological Activity

(A) N1E-115 cells were transfected with wild-type GDE2, GDE2(H233A), GDE2(H275A) or GDE2(C25S) (mCherry-tagged), as indicated. At 24 hr after transfection, cells were stained with phalloidin to visualize F-actin. GDE2 is shown in red, F-actin in green. Bar, 10 µm. **(B)** N1E-115 cells were transfected with wild-type GDE2 or the indicated mutants (mCherry-tagged). At 24 hr after transfection, GDE2 expression was analyzed by immunoblotting using GDE2 antibody. β-Actin was used as loading control. **(C)** Quantification of the morphological changes shown in (A). (Left) Percentage of N1E-115 cells with a round or flattened morphology. (Right) Neurite length quantification. Cells were transfected with pcDNA3 empty vector combined with mCherry as control (three independent experiments with >300 cells per experiment). Error bars, mean ± SEM. *** p value < 0.001; **** p value < 0.0001 of unpaired t-test.

GPC6 Underexpression Phenocopies GDE2 Overexpression and Correlates with Favorable Disease Outcome

We next asked to what extent GPC6 release may account for the biological activity of GDE2, Using SH-SY5Y cells, which express GPC6 as the only relevant glypican (Figure 7A), we established that dox-induced GDE2 expression promotes the release of endogenous GPC6 from the cell surface as measured by flow cytometry (Figure 7B).

GPC6 release from the cell surface predicts loss of GPC6 function. We stably knocked down GPC6 in SH-SY5Y cells by lentiviral transduction of different shRNAs (Figure 7C). GPC6 knockdown cells showed enhanced basal Rac1 activity, which was sensitive to LPA stimulation (Figure 7D), and increased neurite outgrowth (Figure 7E). To validate the knockdown result, we knocked out GPC6 using CRISPR/Cas9-based genome editing (Figure 7F and Figure S5A,B). CRISPR/Cas9-mediated GPC6 knockout led to even more prominent neurite outgrowth than observed with shRNA (Figure 7F). Neurites induced upon GPC6 silencing were fully resistant to LPA-induced contraction (results not shown). In addition, GPC6 depletion resulted in enhanced cell-matrix adhesion and reduced cell motility (Figure 7G,H). It thus appears that loss of GPC6 function is phenotypically equivalent to GDE2 overexpression. We also examined a possible contributing role of GPC3 in regulating neurite outgrowth using cells (IMR-32) that express both GPC3 and GPC6 (Figure S4E,F), but found no effect of GPC3 depletion on neurite formation (Figure S5C,D).

⟶ **Figure 7. GPC6 Silencing Phenocopies GDE2 Overexpression and Correlates with Favorable Outcome**

(A) Glypican mRNA expression (relative to *GAPDH*) in SH-SY5Y cells (qPCR analysis). Error bars, mean ± SEM (trlplicate measurements). **(B)** (Left) Cell-surface expression of GDE2-mCherry before (black) and after (red) doxycycline treatment of SH-SY5Y cells, as detected by Flow Cytometry. (Right) Cell-surface expression of GPC6 in GDE2-negative (black) and GDE2-positive (red) SH-SY5Y cells, as detected by Flow Cytometry. Control or Dox-induced GDE2 cells were labeled with second antibody alone (2^{nd} Ab) or anti-GPC6 antibody. Bar graph shows quantification (mean ± SEM) from three independent experiments. * p value < 0.05 according to paired t-test. **(C)** GPC6 knockdown in SH-SY5Y cells as determined by qPCR. GPC6 mRNA levels were normalized to *GAPDH*. ** p value < 0.01; *** p value < 0.001 of unpaired t-test. **(D)** Western blot showing that GPC6 depletion increases basal and LPA-stimulated Rac activity (SH-SY5Y cells). Bar graph shows quantification of relative Rac-GTP levels in the presence or absence of LPA (mean ± SEM of three independent experiments). * p value < 0.05 of unpaired t-test. **(E)** GPC6 depletion leads to longer neurites (arrows) in SH-SY5Y cells. Bar, 100 μm. Bar graph shows quantification of neurite length in control versus GPC6 knockdown cells (n= 250, mean ± SEM). **** p value < 0.001 of unpaired t-test. **(F)** CRISPR/Cas9-mediated GPC6 knockout promotes neurite outgrowth in SH-SY5Y cells. Bar, 100 μm. Bar graph shows percentage of neurite-bearing cells in CRISPR-GPC6 knockout cells (n ≥ 500 cells, n = 11 colonies, mean ± SEM). **** p value <0.0001. **(G)** shControl and shGPC6 were plated on fibronectin or laminin. At 1 hr after plating, adherent cells were fixed and stained with Crystal Violet for quantification. Bars represent the mean ± SEM of two independent experiments. **(H)** Quantification of average distances of cell migration of shControl and shGPC6 SY5Y cells. Bars represent averages ±SEM (>60 cells). For panels G and H: * p value < 0.05 of unpaired t-test. See also Figure S5.

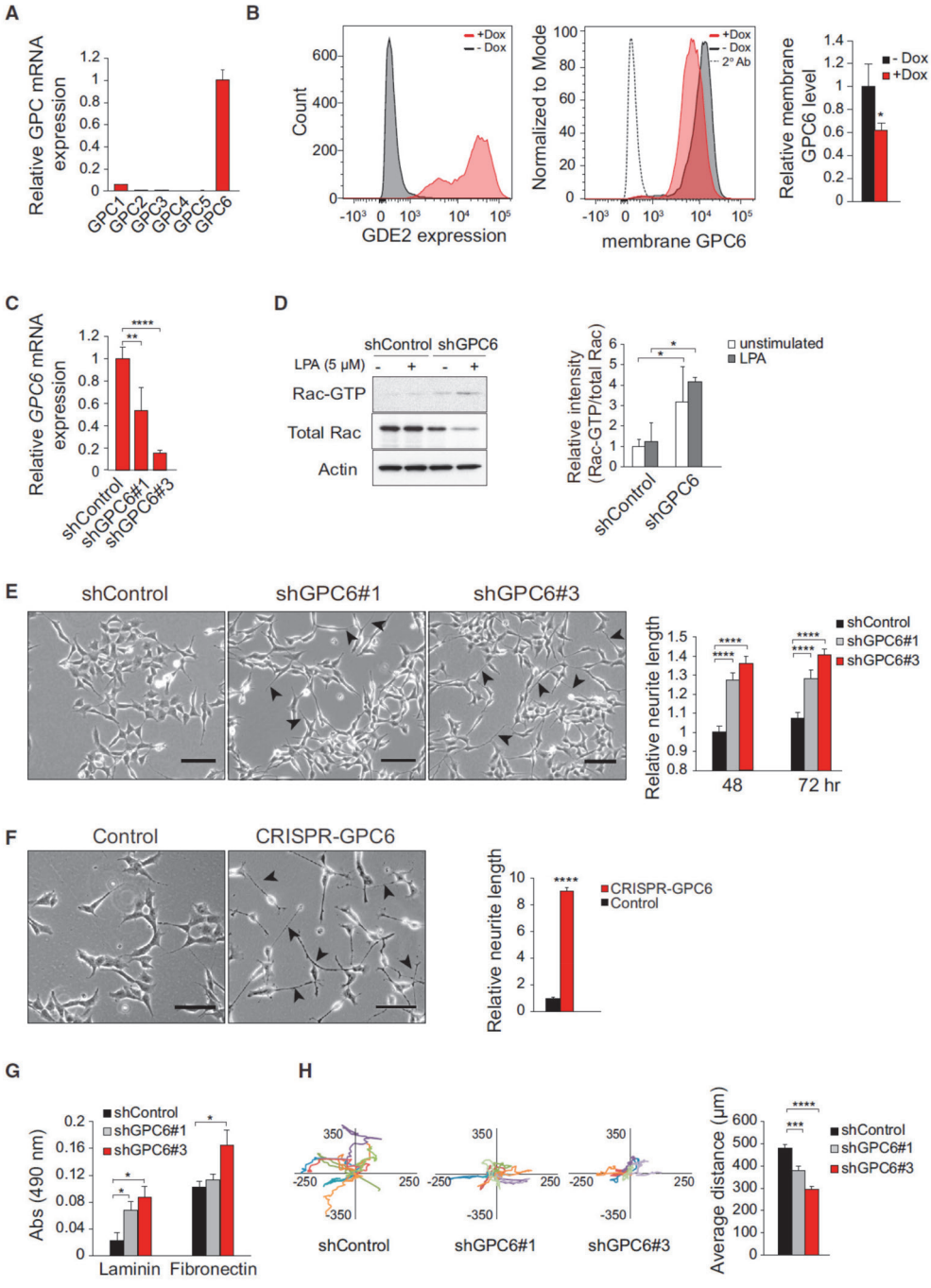
A
Relative GPC mRNA expression
GPC1
GPC2
GPC3
GPC4
GPC5
GPC6
B
+Dox
- Dox
Count
GDE2 expression
+Dox
- Dox
2° Ab
Normalized to Mode
membrane GPC6
Relative membrane GPC6 level
- Dox
+Dox
C
Relative GPC6 mRNA expression
shControl
shGPC6#1
shGPC6#3
D
shControl shGPC6
LPA (5 µM)
Rac-GTP
Total Rac
Actin
Relative intensity (Rac-GTP/total Rac)
unstimulated
LPA
shControl
shGPC6
E
shControl
shGPC6#1
shGPC6#3
Relative neurite length
48
72 hr
F
Control
CRISPR-GPC6
Relative neurite length
CRISPR-GPC6
Control
G
Abs (490 nm)
Laminin
Fibronectin
H
shControl
shGPC6#1
shGPC6#3
Average distance (µm)

Finally, low *GPC6* expression correlated significantly with favorable outcome in neuroblastoma patients (Figure 8A); no significant correlation was found for *GPC3* (Figure S6). When *GDPD5* and *GPC6* expressions were combined, patients classified as *GDPD5*^{high}/*GPC6*^{low} showed the best disease outcome, whereas the *GDPD5*^{low}/*GPC6*^{high} group had the poorest outcome (Figure 8B). This result is consistent with the functional interaction between GDE2 and GPC6 observed in neuroblastoma cell culture.

Discussion

In this study, we have identified and characterized transmembrane ecto-phosphodiesterase GDE2 as an inducer of neuroblastoma differentiation and as a powerful prognostic marker. We find that GDE2, previously shown to promote neurogenesis [108], acts through an enzymatic mechanism involving cleavage of the GPI-anchor of glypican-6 (GPC6). In the simplest model compatible with our findings, GDE2 releases GPC6 from the cell surface to modulate the activity of an as-yet-unknown transmembrane effector (Figure 8C), which leads to Rac activation, suppression of RhoA activity and altered gene expression. Together, these events direct neuroblastoma differentiation as evidenced by neurite outgrowth, increased cell-matrix adhesion, reduced cell motility and blockade of agonist-induced neurite retraction. The set of GDE2-regulated genes was markedly enriched in those involved in neuronal differentiation, cell-matrix adhesion and transmembrane receptor signaling. Future studies should assess whether a subset of these genes contributes to the GDE2-induced phenotypes and/or may represent a gene signature predictive of clinical outcome.

Although GDE2 can also release GPC3, and GPC3 has been implicated in the progression of various types of cancer [191-193], we find that (i) GPC3 is not expressed two of our model neuroblastoma cell lines (SH-SY5Yand N1E-115), (ii) GPC3 knockdown does not affect neurite outgrowth in IMR-32 cells, and (iii) GPC3 expression levels, unlike those of GPC6, do not correlate with clinical outcome. Nevertheless, it will be interesting to explore if and how GDE2-mediated release of GPC3 may regulate signaling pathways and cellular phenotype in other types of cancer or during development.

The cell-autonomous GDE2-GPC6 signaling axis underlying neuroblastoma differentiation contrasts with the non-cell-autonomous GDE2-RECK-Notch pathway that promotes neurogenesis in the spinal cord [109, 110]. Our efforts to detect RECK release [110] by human GDE2 were unsuccessful, suggestive of differential substrate preferences among vertebrates GDE2 enzymes. Moreover, GDE2 was unable to release GPC1, 2, 4 and 5, indicating that GDE2 is highly selective towards GPI-anchored substrates under our experimental conditions. Some caution is needed, however, since the GDE2 activity assays were conducted in HEK293 cells, and the availability of GPI-anchored substrates may depend on local membrane lipid organization and structure [194]. In addition, GDE2 substrate selectivity may be dictated by

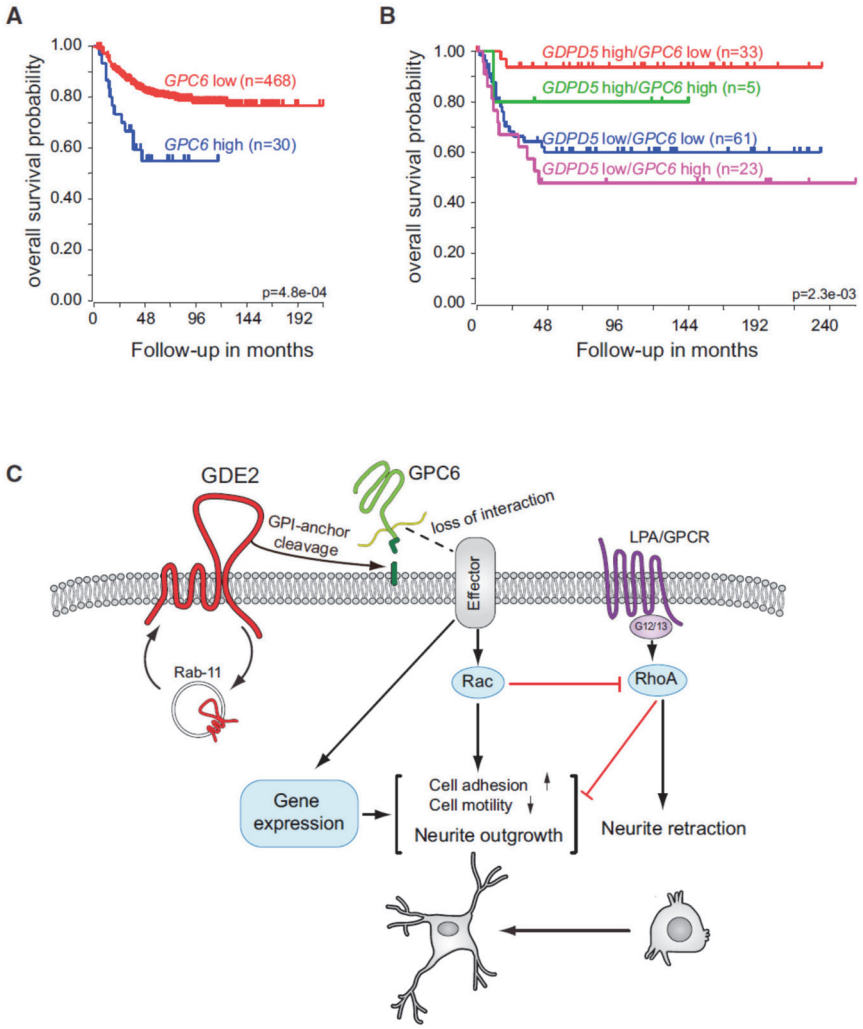

Figure 8. GPC6 Prognostic Significance and GDE2 Signaling Scheme

(A) Kaplan-Meier analysis of overall survival in a set of 498 neuroblastoma patients (RPM cohort). Patients were classified using the same *GPC6* cut-off value. See also Fig. S6. **(B)** Kaplan-Meier analysis based on the combined expression status of *GDPD5* and *GPC6* (AMC patient cohort). **(C)** Proposed GDE2 signaling scheme. In this model, GDE2 acts through GPI-anchor cleavage of GPC6 leading to GPC6 release from the cell surface with consequent loss of interaction with an as-yet-unknown transmembrane effector or receptor. This leads to Rac1 activation, increased cell adhesion and spreading, neurite outgrowth, reduced cell motility, and inhibition of LPA-$G_{12/13}$-RhoA-driven neurite retraction. Additionally, GDE2 regulates a unique set of genes involved in neuronal differentiation, cytoskeletal organization and cell-matrix adhesion (Figure 4I and Table S1). GDE2 cell-surface expression may be regulated by a Rab11-driven endocytic recycling pathway (Figure S1G,H), as illustrated. See text for further details.

structural modifications in the oligosaccharide core of the respective GPI-anchors and/or, in the case of glypicans, by the nature of the heparan sulfate chains which are located close to the cell surface [190] and hence may physically interact with the GDE2 ectodomain. We identified His233 as key catalytic residue of GDE2, but it remains as yet unclear whether GDE2 acts as a PLC- or PLD-type phosphodiesterase [110]. Regardless of how GDE2 selects and hydrolyzes its GPI-anchored substrates, the evidence from the present and previous studies [110] suggests that GDE2 may signal in both cell-autonomous and non-cell-autonomous modes to induce neuronal differentiation, depending on cell and tissue context.

Our findings raise a number of new questions. Foremost of all, how does GDE2-induced cleavage of GPC6 at the cell surface activate downstream signaling events? In other words, what is the GPC6-regulated transmembrane effector? Despite many advances in heparan sulfate proteoglycan research, our understanding of glypican outside-in signaling is still very limited, and that of GPC6 in particular. In fact, GPC6 is the least studied and arguably the most enigmatic glypican family member. Where studied, glypicans can function as co-receptors to regulate transmembrane signaling in various ways, both positively and negatively [188, 195]. As such, certain glypicans can bind specific ligands, including Wnt and Hedgehog proteins, and present them to cognate receptors. However, the emerging picture of glypican-regulated Wnt signaling is complex, involving both canonical and non-canonical signaling cascades, and to date has not led to a unifying model; moreover, findings are sometimes contradictory [196-198]. Whatever possible role of GPC6 in Wnt signaling, the finding that GDE2 acts cell-autonomously, not requiring nearby cells or extrinsic factors, seems hard to reconcile with a role for secreted Wnt ligands in GDE2-induced neuronal differentiation; however, we cannot formally rule out a possible cooperation with secreted ligands such as Wnt.

Interestingly, emerging evidence suggests that glypicans can also function as ligands themselves by binding to transmembrane receptors, namely type-II receptor protein tyrosine phosphatases (RPTPs) [199, 200]. Type-II RPTPs influence neuronal morphology and have multiple intracellular binding partners including regulators of Rac/Rho activity [199, 201]. Heparan sulfate proteoglycans can directly interact (in *cis*) with the ectodomain of RPTPσ to modulate RPTP oligomerization and transmembrane signaling [199, 200]. Loss of a glypican ligand might then lead to altered RPTP clustering at the plasma membrane with a consequent change in localized levels of tyrosine phosphorylated proteins involved in signaling pathways that stimulate neurite outgrowth. Precisely how glypicans in general, and GPC6 in particular, may affect RPTP clustering and activity and whether RPTPs can act as a signaling intermediate in GDE2 action awaits further studies.

Another outstanding question concerns the regulation of GDE2 activity. We could not confirm the proposed role of cytosolic disulfide bonding in regulating GDE2 activity [118, 202]. A relatively large proportion of GDE2 was detected in Rab11- and TrfR-positive recycling endosomes, supporting a model where GDE2 activity is regulated at the level of cell-surface expression by

membrane trafficking (Figure 8C). Interestingly, a recent study supports a scenario in which GDE2 is regulated by intracellular trafficking [119]. Regulation of GDE2 activity by C-terminal tail phosphorylation is another plausible scenario that warrants further investigation [203].

The identification of GDE2 as an inducer of neuroblastoma cell differentiation and as a favorable prognostic marker is consistent with the finding that patient survival is largely dependent on the degree of neuronal differentiation [160]. New therapeutic approaches are urgently needed in neuroblastoma, but their development has been hampered by the paucity of tractable oncogenic drivers [163, 164] and an incomplete understanding of neuroblastoma differentiation. In this respect, the present results open up possibilities for exploring new therapeutic approaches. In particular, pharmacological stimulation of GDE2 activity could be a promising strategy, not least because exo/ecto-phoshodiesterases are convenient drug targets. Therefore, the development of drug-like allosteric activators of GDE2 could be valuable for targeted differentiation therapy in neuroblastoma. Further structural and preclinical studies will be needed to confirm the feasibility and efficacy of this approach.

Experimental Procedures

Human Data Sets and Survival Analysis

All mRNA gene expression analyses were performed within R2: genomics analysis and visualization platform (http://r2.amc.nl). We have made use of the following publicly available data sets: Neuroblastoma Oberthuer (ArrayExpress: E-TABM-38), Neuroblastoma SEQC (GEO:GSE62564) and Neuroblastoma Versteeg (GEO:GSE16476 88/122). Kaplan scanning was performed within R2 (http://r2.amc.nl). In brief, for each gene or other numerical characteristic, R2 calculates the optimal cut-off expression level dividing the patients in a good and bad prognosis cohort. Samples within a data set are sorted according to the expression of the investigated gene and divided into two groups on the basis of a cut-off expression value. All cut-off expression levels and their resulting groups are analyzed for survival, with the provision that minimal group number is eight (or any other user-defined value) samples. For each cut-off level and grouping, the log-rank significance of the projected survival was calculated as described [204]. The best p value and corresponding cut-off value is selected. This cut-off level is reported and used to generate Kaplan-Meier graphs.

Materials, Cell Culture, Antibodies and Expression Vectors

Reagents, cell culture, expression vectors and transfection protocols are described in Supplemental Information. A GDE2 polyclonal antibody was raised against the very C-terminal tail of human GDE2 (sequence MVRHQPLQYYEPQ) and affinity purified, as described in Supplemental Experiment Procedures.

Cell Morphology and Neurite Induction
Phenotypic analyses were done as described in Supplemental Experiment Procedures.

Gene Silencing
shRNA-mediated knockdown and CRISPR/Cas9-mediated knockout experiments were performed as described in Supplemental Experiment Procedures.

Differential Gene Expression by RNA-seq
Differential gene expression in GDE2 knockdown versus control Shep2 cells was analyzed by whole-genome RNA sequencing (RNA-seq) as described in Supplemental Procedures.

qRT-PCR and Western Blotting
Real-time PCR and Western blotting assays were carried out as described in Supplemental Procedures.

Microscopy and Live Imaging
Confocal and super-resolution microscopy assays and live-imaging protocols are described in Supplemental Procedures**.**

Cell Adhesion and Motility Assays
Cell adhesion and random cell motility were measured as detailed in Supplemental Procedures.

GDE2 Enzymatic Activity Assays
GDE2 activity assays were carried out in HEK293 cells, essentially as described [110]. HEK293 cells were seeded on polyethyleneimine (PEI)-coated 6-well plates and co-transfected with expression vectors for chicken or human GDE2 together with substrates (RECK-Myc, GPC(1-6)-HA). GDE2 mutations were made using X-tremeGene 9 reagent (Roche). At 24 hr after transfection, cells were incubated for an additional 24 hr in serum-free DMEM. The conditioned medium was removed and cell lysates were prepared using NP40/NaDOC lysis buffer (50 mM TRIS ph7,4, 150 mM NaCl, 2mM EDTA, 1% NP40, 0,25% NaDOC and 5% Glycerol) supplemented with protease inhibitor cocktail. The amount of substrate proteins in the medium and cell lysates was analyzed by Western blotting.

Rac and RhoA Activity Assays
Activities of Rac and RhoA were measured by pull-down assays as described in Supplemental Experimental Procedures.

RhoA Activation Measurements

To monitor RhoA activity in real time, cells were transfected with a RhoA-specific FRET-based biosensor in which the HR1 region of protein kinase N was used as the effector domain for activated RhoA, essentially as described [187]. Further details and RhoA activity monitoring in single cells are described in Supplemental Experimental Procedures.

Acknowledgements

We thank Laurens van Meeteren, Paula Ruurs, Maikel Jongsma and Andrew J. Morris for performing pilot experiments, Bram van de Broek for image analysis and Elisabetta Argenzio

Supplemental Experimental Procedures

Cell Culture and Materials

SH-SY5Y, IMR-32, Shep2, N1E-115, Neuro2A and HEK293 cells were grown in Dulbecco's modified Eagle's medium (DMEM) supplemented with 10% fetal bovine serum (FBS) at 37°C under 5% CO2. Antibodies used: anti-HA, 3F10 from Roche Diagnostics; anti-Flag, M2 and β-Actin (AC-15) from Sigma; RECK (D8C7) from Cell Signaling Technology; anti-RhoA (26C4) (sc-418) from Santa Cruz; anti-Rac1 from BD Transduction Laboratories; anti-GPC6 from LSBio; anti-mCh and anti-GFP were home-made; 1-oleyl-LPA, puromycin, fibronectin, laminin-1, collagen and doxycycline were from Sigma. Bacterial PI-PLC was from Molecular Probes and Phalloidin red (actin-stain™ 555 phalloidin) from Cytoskeleton.

GDE2 Antibody Generation

GDE2 polyclonal antibody against the C-terminal 14 amino acids of human GDE2 (GGSHTKTLIERSGR) was raised in rabbits. The peptide was fused to mcKLH (Keyhole limpet hemocyanin; Pierce) in conjugation buffer (0.1 M Sodium phosphate, 0.15 M NaCl, pH 7.2; Pierce Kit) and then purified by a desalting column (Pierce Kit). For affinity purification, the antiserum was passed through a GDE2 peptide column, and the cross-absorbed serum was affinity purified using the Aminolink®Plus Immobilization Kit (Thermo Scientific).

Expression Vectors

Human cDNA GDE2 was subcloned into a pcDNA3 (-mCherry and –EGFP) plasmid by amplification with oligos and digestion was done with BamHI/EcoRV. GDE2 mutants (C25S, H233A, H275A and H233/275A were made by site-directed mutagenesis followed by Dpn1 digestion of the template. The viral plasmid pLIB-GDE2-GFP was constructed by subcloning the insert containing two mutations in residues 1731 and 1734 into pLIB vector. Constructs pCAGGS-HA-GPC1-6, pCAGGS-cGDE2-Flag, pCAGGSMyc-RECK were kindly provided by Dr. Sungjin Park (Johns Hopkins Medical School, Baltimore, USA).

Inducible GDE2 Expression

SH-SY5Y and IMR-32 cells with inducible GDE2 expression were generated using the Retro-X™ Tet-On® Advanced Inducible Expression System (ClonTech). After retroviral transduction, the cells were placed under selection with G418 (800 mg/ml) supplemented with puromycin (1 mg/ml) for 10 days. GDE2 induction (in the presence of 1 μg/ml doxycycline) was verified by Western blot and confocal microscopy.

Cell Morphology, Neurite Induction and Retraction

For quantification of cell morphology, cells were transiently transfected with GDE2, GDE2(H275A), GDE2(H233A), GDE2(H233/H275A) or GDE2 (C25S) (all mCherry-tagged). At 24h post-transfection, cells were fixed with 4% paraformaldehyde and F-actin was stained with phalloidin. Cells were visualized using an inverted Leica confocal microscope. Per experiment, ~300 cells were randomly scored as round or flat, or round or cells bearing neurites. For neurite length measurements, cells were seeded at 1x 10^5 cells/well in 6-well plates. GDE2 expression was induced by addition of 1 µg/ml doxycycline in DMEM containing 4% serum for 72 hr. Pictures were taken at 48 and 72 hr to monitor neurite outgrowth. Neurite length was measured using an Image J macro. Differentiated cells were defined as those with neurite lengths exceeding one cell-body diameter. Experiments were performed in triplicate. For quantification of neurite retraction, N1E-115 cells were serum starved for 24 hr and then treated with LPA. Next, cells were fixed and stained with phalloidin. Per time point, about 300 randomly selected cells were scored as round or flat.

Cell Adhesion and Motility

Cell adhesion and random cell motility were measured using standard procedures. For adhesion assays 96-well plates were coated at 37 °C with 10 µg/ml fibronectin, 5 µg/ml collagen or 10 µg/ml laminin-1 during 1hr. The plates were washed with PBS, blocked in 0.5% BSA for 1hr at 37 °C and washed twice with PBS. Cells were seeded at 1x10^5 per well and allowed to adhere at 37 °C for 1 hr. Non-adherent cells were washed away using PBS. Attached cells were fixed with 4% paraformaldehyde (PFA) for 10 min, washed twice and stained with crystal violet (5 mg/ml in 2% ethanol) for 10 min. Fixed cells were washed and lyse with 2% SDS for 30 min. Plates were read at 490 nm. To measure random cell motility, cells were seeded on fibronectin-coated 6-well plates in the presence of serum 24 hr earlier. Phase-contrast images were acquired using a Zeiss Axiovert 200M microscope equipped with a heated (37°C) chamber and CO2 controller. Images were taken every 10 min during 12 hr, and the distance covered by the cells and cell directionality were analyzed using ImageJ software.

Expression Profiling

The mRNA expression profile of 24 established neuroblastoma cell lines was established by microarray using the Affymetrix Human Genome U133 plus 2.0 platform. Expression data are deposited at GEO (accession number GSE28019).

Knockdown Studies

For knockdown studies, we used five independent shRNAs for each gene in the lentiviral vector pLKO, as listed below. To generate particles for stable infections, HEK293T cells were transfected with single shRNAs using the calcium phosphate protocol; the virus particles

were collected at 48 h after transfection. Stable GDE2 knockdown cells were selected and maintained in medium containing 2 μg/ml puromycin. For imaging studies, plasmids were transiently transfected using XtremeGene 9 agent (Roche) according to the manufacturer's instructions.

Gene	TRC ID	Full hairpin sequence
GDPD5	TRCN0000005173	CCGGCCTGGTAGAAGTGTTCTGGATCTCGAGATCCAGA ACACTTCTACCAGGTTTTT
	TRCN0000005174	CCGGGCTCTCCGTATGTTCAGACAACTCGAGTTGTCTGA ACATACGGAGAGCTTTTT
	TRCN0000005175	CCGGCCACAATGACTATGATGAATTCTCGAGAATTCATCA TAGTCATTGTGGTTTTT
	TRCN0000005176	CCGGGACAACAGTTATGACACATATCTCGAGATATGTGTC ATAACTGTTGTCTTTTT
	TRCN0000005177	CCGGGTCCTGGCACTATGTCACATTCTCGAGAATGTGAC ATAGTGCCAGGACTTTTT
GPC6	TRCN0000123094	CCGGGCTTCCTCTTTCCTTCAGCTACTCGAGTAGCTGAA GGAAAGAGGAAGCTTTTTG
	TRCN0000123095	CCGGGCCATTATGAACATGCAAGAACTCGAGTTCTTGCA TGTTCATAATGGCTTTTTG
	TRCN0000123096	CCGGGCCAACAAAGCAAACTCGAATCTCGAGATTCGAG TTTGCTTTGTTGGCTTTTTG
	TRCN0000123097	CCGGGCACAGCAAAGCCAGATACTTCTCGAGAAGTATC TGGCTTTGCTGTGCTTTTTG
	TRCN0000123098	CCGGACCCGATAGATGTCAAGATTTCTCGAGAAATCTT GACATCTATCGGGTTTTTTG
GPC3	TRCN0000078558	CCGGGCCAAATTATTCTCCTATGTTCTCGAGAACATAGGA GAATAATTTGGCTTTTTG
	TRCN0000078559	CCGGCCTGAAAGTATTTGGGAATTTCTCGAGAAATTCCC AAATACTTTCAGGTTTTTG
	TRCN0000078560	CCGGCCCATTCTCAACAACGCCAATCTCGAGATTGGCGT TGTTGAGAATGGGTTTTTG
	TRCN0000078561	CCGGGCTCTGGTGATGGAATGATAACTCGAGTTATCATTC CATCACCAGAGCTTTTTG
	TRCN0000078562	CCGGGCCTGTTTCCAGTCATCTATACTCGAGTATAGATGA CTGGAAACAGGCTTTTTG

CRISPR/Cas9-mediated GPC6 Knockout

SH-SY5Y *GPC6* knockout cell lines were generated using CRISPR/Cas9 genome editing. CRISPR sequences were designed to target *GPC6* (exon 2: 5'-AATGGCTTGTCTCTTCCACA-3'; exon 3: 5'-GCTGAAAAGGTACTACACTG-3') and cloned into pX330-eSpCas9(1.1) [205].

SH-SY5Y cells were transfected with the exon-specific pX330-eSpCas9(1.1) plasmids in addition to a plasmid containing a guide RNA to the zebrafish TIA gene (5'-ggtatgtcgggaacctctcc-3') plus a cassette of a cytomegalovirus promoter followed by a BlastR gene, flanked by two TIA target sites. Co-transfection results in infrequent integration of the BlastR gene at the targeted genomic locus by NHEJ, as previously described [155]. Successful integration of the cassette renders cells resistant to blasticidin. At seven days after transfection, the culture medium was supplemented with blasticidin (10 µg/ml). Surviving colonies were clonally expanded, screened for cassette integration and indels into the query gene by PCR (using primer sets 5'-GGGGAACACTTAAGAATCTGTCC-3' and 5'-CTTATGCCTGGACACAAAAGTG-3' and 5'- AGCTCCTGGAGAATGCAGAA-3' and 5'- GAAGTGATACTGAGGGTTTATCAGC-3' for exon 2 and 3, respectively). Plasmid SpCas9(1.1) was kindly provided by Feng Zhang (Addgene plasmid # 71814) and pTIA-CMV-BlastR by Thijn R. Brummelkamp.

qRT-PCR

Total RNA was extracted using the GeneJET purification kit (Fermentas). cDNA was synthesized by reverse transcription from 2 µg RNA using oligodT 15 primer and SSII RT enzyme (Invitrogen). RTqPCR was performed on a 7500 Fast System (Applied Biosystems) as follows: 95°C for 2 min, 95 °C for 0 min., 40 cycles at 95°C for 15 sec. followed by 60°C for 1 min. for annealing and extension. The final reaction mixtures (20 µl) consisted of diluted cDNA, 16SYBR Green Supermix (Applied Biosystems), 200 nM forward primer and

Gene	Forward primer 5'-3'	Reverse primer 5'-3'
GDPD5	GTACCTCTACAACCGCATGG	AATGTGACATAGTGCCAGGAC
GPC1	GATGACCACTTCCAGCACCT	CAGGTAGTCATCAGGCAGCA
GPC2	TGAGACAGAGCAGAGGCTGA	AGAGCTGGGTCAGAGAGTGC
GPC3	TGCTCTTACTGCCAGGGACT	GCTTTCCTGCATTCTTCTGG
GPC4	TTCGAGTGATGACCAGCAAG	AGCACTGTCGGCTTTCTCAT
GPC5	CAGTGGGGACTGTGATGATG	ACCAAATCCCGGGAAGTAAC
GPC6	CAACATTGAGTCGGTCATGG	ATTGTAGGGCCTGAAACGTG
GAPDH	GCCAAGGTCATCCATGACAAC	GAGGGGCCATCCACAGTCTT
MAP2	CCAATGGATTCCCATACAGG	TCCTTGCAGACACCTCCTCT
TUBB3	CCTGGAACCCGGAACCAT	AGGCCTGAAGAGATGTCCAAAG
ENO2	CTGATGCTGGAGTTGGATGG	CCATTGATCACGTTGAAGGC
SNAP25	AGTTGGCTGATGAGTCGCTG	TGAAAAGGCCACAGCATTTC
NEUROD1	CCGACAGAGCCCAGATGTAGTTCTT	GCCCCAGGGTTATGAGACTATCACT
GAP43	GAGGATGCTGCTGCCAAG	GGCACTTTCCTTAGGTTTGGT
NPY	TACCCCTCCAAGCCGGACAA	CATTTTCTGTGCTTTCTCTCAT
PPIA	CATCTGCACTGCCAAGACTGA	TTGCCAAACACCACATGCTT

200 nM reverse primer. Reactions were performed in 96-well plates in triplo. The primers used are listed below. As a negative control, the cDNA was replaced by milliQ. GAPDH and Cyclophilin , were used as reference genes. Each sample was analyzed in triplo. The normalized expression (NE) data were calculated by the equation $NE = 2^{(Ct\ target\ -\ Ct\ reference)}$.

Western Blotting

For Western blotting, cells were washed in ice-cold PBS, lysed in RIPA buffer with protease inhibitors and spun down. Equal amounts of proteins were determined by BCA protein assay kit (Pierce), separated by SDS-PAGE using pre-cast gradient gels (4-12% Nu-Page Bis-Tris, Invitrogen) and transferred to nitrocellulose membranes. Nonspecific binding of proteins was blocked by incubation in 5% skimmed milk in TBST. Proteins were detected by 1 hr incubation of primary antibody at room temperature or overnight incubation at 4°C, followed by 1 hr incubation with horseradish peroxidase-conjugated secondary antibodies (DAKO, Glostrup, Denmark). Proteins were detected using ECL Western blot reagent (GE Healthcare, Chalfont St. Giles, UK).

Immunofluorescence

Cells were cultured on glass coverslips, fixed with 4% paraformaldehyde for 10 min, permeabilized by 0.1% Triton X-100 and subsequently blocked in 2% BSA for 30 min at room temperature. Incubation with primary antibody was done for 1hr and coverslips were then incubated with Alexa-conjugated secondary antibodies for 45 min at room temperature. Cells were washed with PBS before mounting with Immuno-Mount™ (Thermo Scientific). Slides were examined on a LEICA TCS-SP5 confocal microscope (63x objective).

Live-Cell Imaging

Live-cell imaging was done on a Leica TCS SP5 confocal microscope equipped with 63x oil immersion lens (numerical aperture 1.4; Leica, Mannheim, Germany). Coverslips were mounted in a metal ring system and exposed to buffer solution (140 mM, NaCl, 5 mM KCl, 2 mM MgCl2, 1 mM CaCl2, 23mM NaHCO3, 10 mM HEPES, 10 mM glucose). Cells were selected randomly. LPA was added while images were collected at appropriate time intervals (5-15 sec). GDE2-mCherry was visualized by exciting cells at 561 nm while emission was detected at 610 ± 10 nm.

Super-Resolution Microscopy

Cells were cultured on #1.5 uncoated coverslips and washed with PBS and fixed with 4% paraformaldehyde. Imaging was done on a SR-GSD [206] Leica microscope, using an oxygen scavenging system (GLOX: 10% glucose, 0.5 mg/ml glucose oxidase, 40 µg/ml catalase) with the reducing agent MEA (cysteamine hydrochloride, 100 mM). Images were taken in TIRF or EPI mode at 10 ms exposure time for 15000 frames. Post image analysis was performed

as follows: a temporal median filter was applied on the blinking movies to reduce structured background [207] using home-built software. The resulting movies were analyzed with the ImageJ plugin Thunderstorm (http://imagej.nih.gov/ij/) for blinking localizations, XY drift correction and construction of the final image, which were made with Normalized Gaussian visualization option (pixel size 20 nm). Chromatic aberration was corrected using 0.1 µm diameter Tetraspec microsphere (Invitrogen) images from which an affine transformation matrix was constructed. Correction of all images was performed with an ImageJ macro using the plugin Image Stabilizer.

Flow Cytometry

For GPC6 surface expression analysis, cells were grown in complete medium with 10% FCS with or without doxycycline. Cells were trypsinized into single-cell suspensions and then $8x10^5$ cells were incubated with 7 µl of anti-GPC6 antibody LS-C36518 (LifeSpan Bioscience). Bound antibodies were detected by incubating with a 1:200 dilution of goat anti-mouse Alexa-488 secondary antibody in 2% BSA for 45 min on ice. Fluorescence measurements were performed using BD LSRFORTESSA and using Flow Jo software.

Rho GTPase Activity Assays

Rac1 and RhoA GTPase activities were assayed as described previously (Sander *et al*., 1999). Briefly, cells were gradually cooled on ice, washed with cold PBS (containing 1mM CaCl2, and 0.5mM MgCl2+) and lysed with a lysis buffer containing 0.5% Nonidet P-40, 10mM Tris, 150 mM NaCl, 50 mM MgCl2, protease inhibitor and 2 µg/ml PAK-CRIB peptide [208] or GST-Rhotekin (Sander et al., 1999). Cell lysates were cleared by centrifugation, and cleared supernatants were added to washed streptavidin beads (Rac-PAK-CRIB) or with glutathione beads (Rho-GST-Rhotekin), solubilized in SDS sample buffer and rotated for 30 min. at 4oC. Beads were washed and bound proteins were taken up in sample buffer (NuPage, Invitrogen) and used for Western blot analysis.

RhoA Activation in Real-Time

RhoA activity was monitored in real-time using a RhoA-specific FRET-based biosensor, as previously described (Kedziora et al., 2016). A FRET pair consisting of Cerulean3 and circularly permutated Venus was used. The HR1 region of PKN was used as the effector domain for activated RhoA. Cells were transfected with the biosensor and assessed for RhoA activation by LPA. GDE2-mCherry or mCherry-CAAX was co-transfected. At 48 hr after transfection, coverslips were mounted in an imaging ring and transferred to an inverted wide-field microscope (Nikon) equipped with a heated 63x, oil immersion objective. Excitation was at 425 nm and acceptor (CFP) and donor (Venus or YFP) emission was detected at the same time at 470±20 nm and 530±25 nm, respectively. FRET was expressed as the ratio of acceptor to donor emission.

RNA Sequencing and Bioinformatics

RNA from Shep2 knockdown and shControl Shep2 cells was extracted and subjected to RNA sequencing (RNA-seq) at the NKI Genomics Core Facility. The reads (65bp single-end) were sequenced on a Illumina HiSeq-2500 platform and mapped to the human reference genome (hg38) using TopHat (version 2.0.12) [209], which allows to span exon-exon splice junctions. TopHat was supplied with a known set of gene models, the transcriptome-index parameter (Ensembl version 77). The samples were generated using a stranded protocol, meaning that TopHat was guided to use the first strand as the library type. Tophat was run with bowtie 1 version 1.1 and uses the prefilter-multihits and no coverage as additional arguments. To count the number of reads per gene, a custom script (Itreecount) was used, which is based on the HTSeq-count [210] and has comparable output. Itreecount generates a list of the total number of uniquely mapped sequencing reads for each gene that is present in the provided Gene Transfer Format (GTF) file. Differential expression was performed using the R package Limma. Limma contains the Voom method [211], which normalizes to log2 counts per million reads per sample and corrects for the library size of each sample. After data transformation, differential expression was analyzed. Samples were compared against each other using the standard Limma pipeline. This provided log2-fold changes and p-values corrected for multiple testing. A gene was considered differentially expressed if the p-value < 0.05. All raw sequence data are deposited at GEO (accession number GSE74345).

Supplementary figures

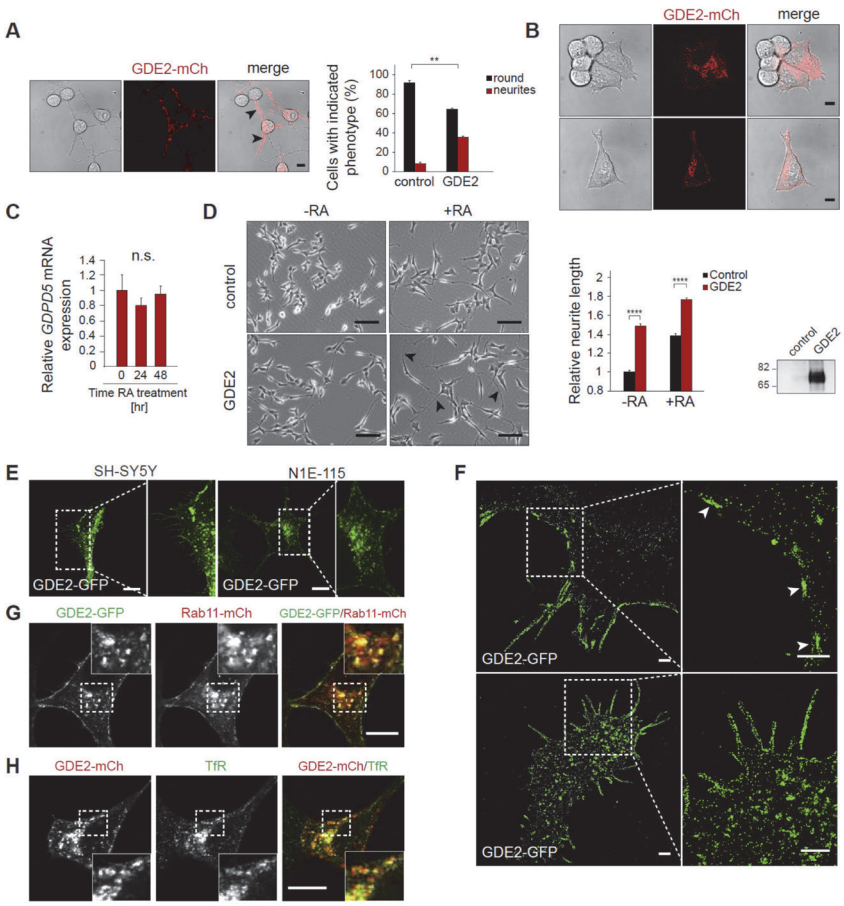

Figure S1. GDE2: morphological changes and subcellular localization. Related to Figure 2. **(A)** (Left) GDE2-induced neurite outgrowth (black arrows) in Neuro-2a cells expressing GDE2-mCh. Bar, 10 μm. (Right) Quantitative analysis of "round" or "neurite-bearing" morphologies of GDE2-overexpressing cells versus control cells (n= 300 cells, mean ± SEM). ** p value < 0.01 (Fisher's test). **(B)** Cell spreading in contacting and isolated N1E-115 cells expressing GDE2-mCh. Bar, 10 μm. **(C)** *GDPD5* expression (relative *to GAPDH*) in SH-SY5Y cells treated with retinoic acid (RA, 2 μM) for 0-48 hr (qPCR analysis). Error bars, mean ± SEM (triplicate measurements); n.s. not significant. **(D)** (Left) Neurite formation in control and GDE2-overexpressing SH-SY5Y cells in the absence or presence of RA (2 μM; 48 hr). (Right) Quantification of neurite outgrowth (n= 250 cells; mean ± SEM). **** p value < 0.0001 (unpaired t-test). GDE2 was detected using anti-GDE2 antibody. **(E)** Localization of GDE2-GFP in the indicated cell lines. Bar, 10 μm. **(F)** Localization of GDE2-GFP in N1E-115 cells as detected by super-resolution microscopy. White arrows point to distinct microdomains at the plasma membrane. Bar, 1 μm. **(G)** Localization of GDE2-GFP and Rab11-mCh in N1E-115 cells. Bar, 10 μm. **(H)** Localization of GDE2-mCh and endogenous transferrin receptor (TfR) in Dox-induced SH-SY5Y cells. Bar, 10 μm.

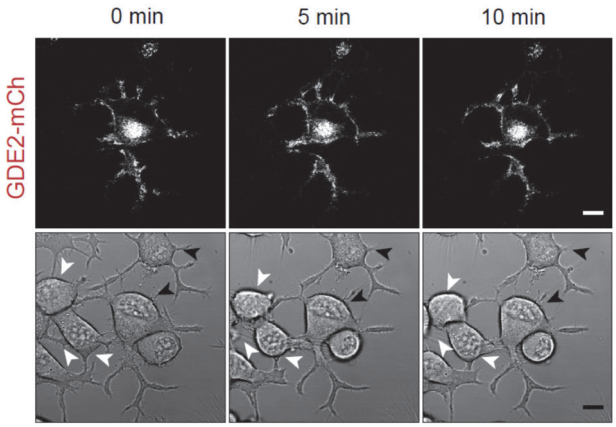

Figure S2. Inhibitory effect of GDE2 on neurite retraction by LPA. Related to Figure 3
N1E-115 cells were transfected with GDE2-mCh and stimulated by LPA (1 μM) for the indicated times. GDE2-mCh-expressing cells are indicated by black arrows, non-transfected cells by white arrows. See also Supplemental Movie S1 and S2.

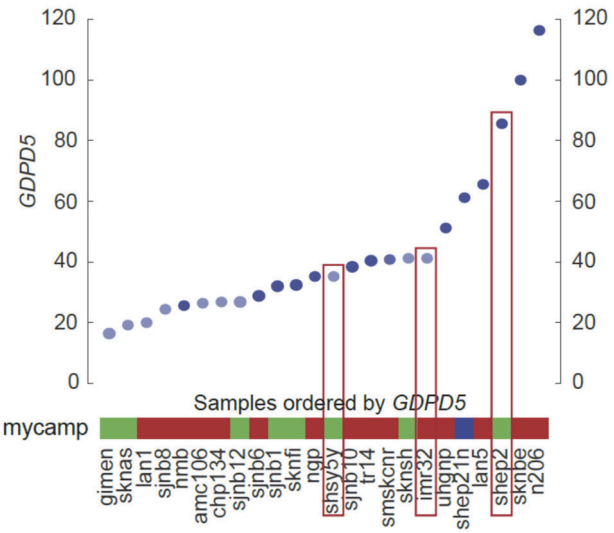

Figure S3. *GDPD5* expression in neuroblastoma cells. Related to Figure 4
GDPD5 expression in 24 different human neuroblastoma cell lines (microarray analysis); mycamp denotes *MYCN* amplification status. Shep2 cells were selected for knockdown studies.

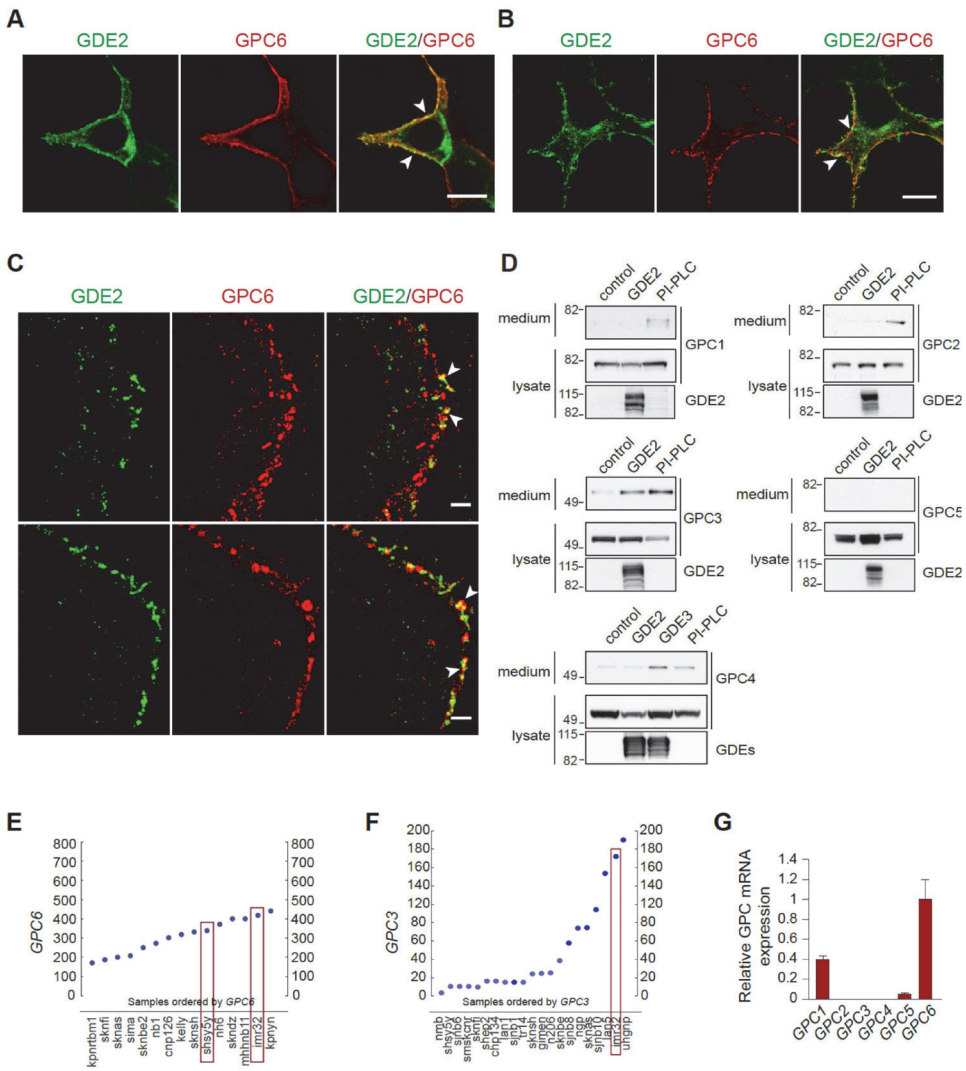

Figure S4. Glypican expression and GDE2-induced release. Related to Figure 5

(A,B) Confocal images of HEK293 cells (A) and N1E-115 cells (B) co-expressing GDE2-GFP and GPC6-HA. White arrows point to distinct microdomains (yellow) showing overlapping localization. Bar,10 μm. **(C)** Dual-color super-resolution images of N1E-115 cells co-expressing GDE2-GFP and GPC6-HA. White arrows point to distinct microdomains (yellow) showing overlapping localization. Bar, 1 μm. **(D)** HEK293 cells were co-transfected with GDE2-mCh and the indicated glypicans (HA-tagged). Glypican levels were assessed by immunoblotting of conditioned medium and cell lysates and. PI-PLC was used as positive control. **(E)** *GPC6* expression in the indicated neuroblastoma cell lines (microarray analysis). **(F)** *GPC3* expression in the indicated neuroblastoma cell lines (microarray analysis). **(G)** *GPC1-6* expression (relative to *GAPDH*) in N1E-115 cells (qPCR analysis). Error bars, mean ± SEM (triplicate measurements).

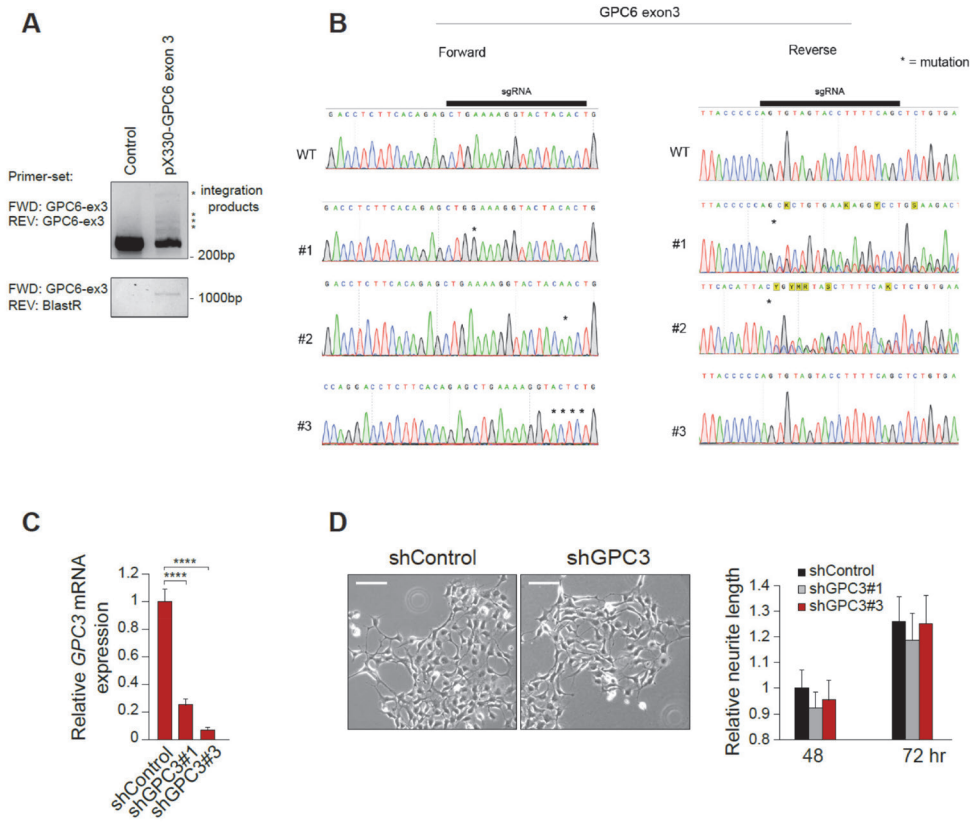

Figure S5. Validation of *GPC6* knockout in SH-SY5Y cells and assessment of GPC3 depletion in IMR-32 cells. Related to Figure 7

(A) *GPC6* knockout in SH-SH5Y cells was achieved using CRISPR/Cas9 genome editing. The panel shows incorporation of the BlastR gene as measured by PCR amplification of genomic DNA. **(B)** Sanger sequencing from clones targeted with CRISPR/Cas9 for GPC6 exon3. **(C)** *GPC3* mRNA expression (relative to *Cyclophilin A*) in control and GPC3-depleted IMR-32 cells, using two different shRNAs against GPC3. Errors bars, mean ± SEM; **** p value < 0.0001 (unpaired t-test). **(D)** (Left) IMR-32 cell morphology before and after GPC3 depletion. Bar, 100 μm. (Right) Quantification of neurite outgrowth in control and GPC3-depleted IMR-32 cells after 48 and 73 hr (n = 200 cells; mean ± SEM; differences

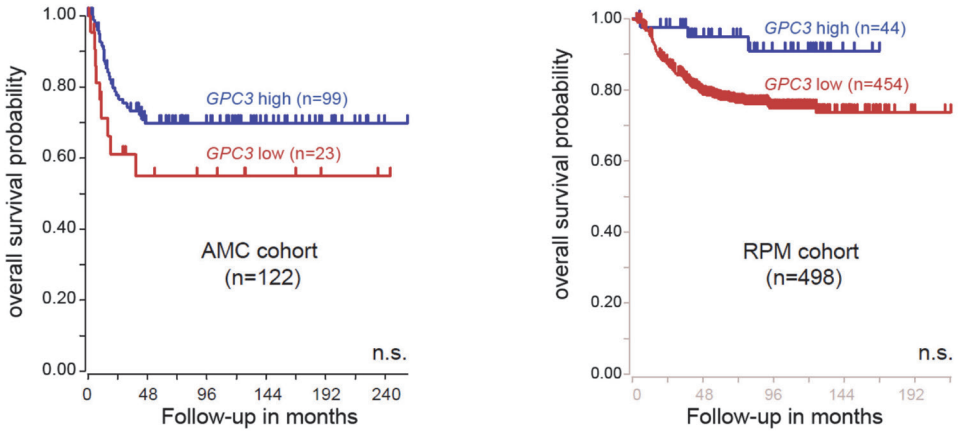

were not statistically significant).

Figure S6. *GPC3* expression and patient survival probability. Related to Figure 8
Kaplan-Meier analyses of *GPC3* expression versus overall survival in the indicated neuroblastoma patient cohorts.

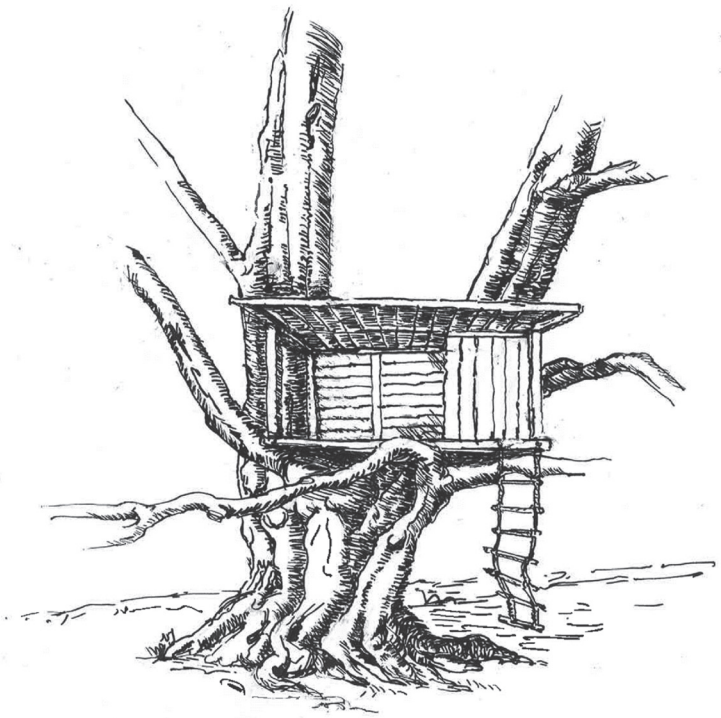

FAGUS SYLVATICA

Addendum Chapter 3

Neuronal differentiation through GPI-anchor cleavage

Adapted from: Oncotarget 2017;8:5672–5673 and Cell Cycle 2017;16:388-389

Elisa Matas-Rico, Michiel van Veen, Wouter H. Moolenaar
Division of Cell Biology, The Netherlands Cancer Institute, Amsterdam, Netherlands

Introduction

The cell surface of virtually all cell types harbors a great variety of Glycosylphosphatidylinositol (GPI)-anchored proteins with diverse biological functions. GPI-anchoring is a complex post-translational modification that anchors proteins in the outer leaflet of the plasma membrane [146]. GPI-anchoring may allow for lateral movement and some structural flexibility of membrane proteins, but otherwise the biological function of GPI anchors has long remained a mystery. Some GPI-anchored proteins are released from their anchor and detected in body fluids and cerebral fluid, implying involvement of putative GPI-specific phospholipases. But the mechanism and physiological significance, if any, of GPI-anchor cleavage has long remained unexplored. Recent studies have advanced the field by showing that selective cleavage of GPI-anchored proteins by an ecto-phosphodiesterase, termed GDE2, leads to neuronal differentiation [110, 137]. GDE2 (encoded by *GDPD5*) is a member of the glycerophosphodiesterase family [96] and characterized by six transmembrane domains and a large catalytic ectodomain. Since GDE2 hydrolyzes distinct substrates to promote neural differentiation, it will be important to explore the substrate selectivity of GDE2 in further detail and also that of its close relative GDE3 [96]. Here we focus on the nervous system since multiple GPI-anchored proteins are known to participate in the development and proper functioning. In fact, in humans, most germline mutations in the GPI-anchor synthesis pathway are presented with mental retardation phenotypes, underlining the importance of proper regulation of GPI-APs during neural development [212, 213]. Hence, comprehending the function and release of GPI anchored proteins in the nervous system could be indicative in finding new roles for GDE's.

GPI anchor release by GDEs

GDE2 was originally identified as a retinoic acid-inducible gene that promotes spinal motor neuron differentiation by inhibiting Notch signaling in adjacent neuronal progenitors [109]. Mechanistically, the Notch transmembrane receptor is activated by binding membrane-bound ligands on contacting cells. GDE2 was reported to cleave and release a GPI-anchored Notch regulator, termed RECK, that normally inhibits protease-dependent shedding of a Notch ligand [110]. By releasing RECK, GDE2 inactivates the ligand-Notch signaling axis and thereby promotes differentiation in contacting neuronal cells (**Fig.1**). Thus, in the developing spinal cord, GDE2 promotes neurogenesis in a non-cell-autonomous manner, requiring cell-cell contact [110]. Coherent with the previous findings we found that GDE induces neuroblastoma differentiation (Matas et al., 2017). Neuroblastoma is a highly heterogeneous disease, characterized by relatively few recurrent somatic mutations [214]. Some high-risk neuroblastomas are associated with mutations in Rho GTPase pathway genes that normally regulate the differentiated phenotype and are implicated in neuritogenesis and cell motility

[163]. Through overexpression and knockdown studies, GDE2 was found to change the Rac-RhoA activity balance leading to cell spreading, neurite outgrowth, inhibition of RhoA-driven neurite retraction and reduced cell motility in both mouse and human neuroblastoma cells. To our surprise we discovered that GDE2 does so through GPI-anchor cleavage of the heparan sulfate proteoglycan glypican-6 (GPC6) in a cell-autonomous manner, not requiring cell-cell contact [137] (**Fig.1**). It is of note that GDE2's closest family member GDE3, also cleaves GPC6 (and other GPI-anchored proteins) and is expressed in the nervous system, although its function there is unknown [17, 110]. Altogether these data suggest that GDE2 initiates a neuronal differentiation program and that understanding GPI-anchor release in the neuronal system may hint towards a possible role for other GDE's in general.

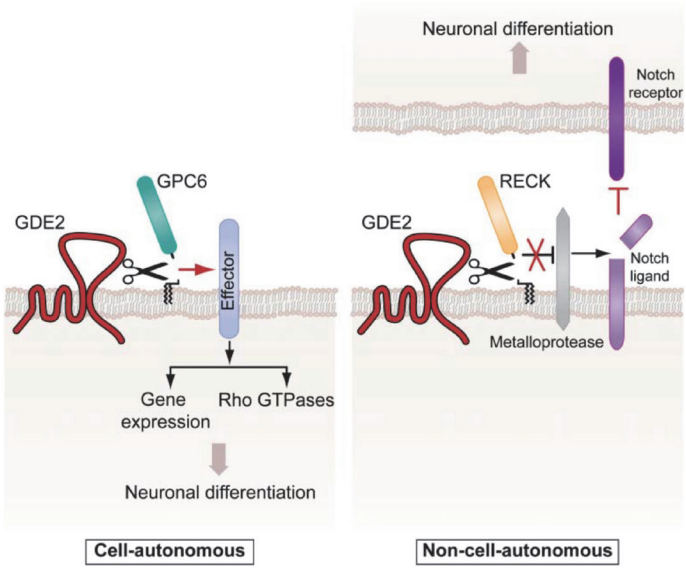

Figure 1. GDE2 cleaves GPI-anchored substrates to promote neuronal differentiation in distinct manners

Left panel, GDE2-induced cleavage of glypican-6 (GPC6) signals differentiation of neuroblastoma cells, involving both Rho GTPase-driven cytoskeletal remodeling and new gene transcription. Right panel, RECK cleavage is a trigger to downregulate Notch signaling in adjacent neural progenitors. It is unclear if GDE2 acts as a PLC or PLD.

GPI-anchored proteins in the nervous system

Glypicans

During neuronal development and normal homeostasis GPI-anchored proteins serve an important function as co-receptors and ligands of various signaling pathways. In fact, the

frequent occurrence of GPI-anchored proteins in the nervous system suggests a common underlying function, possibly being regulated release. One such protein family, glypicans, are indeed secreted in the nervous system. However, their soluble role remains largely unknown. Glypicans belong to the larger family of proteoglycans that are all composed of a core protein to which glycosaminoglycan side chains (GAGs) are attached. In vertebrates, GPCs play key roles during normal neuronal development [70, 215, 216], but are also associated with neurofibrillary tangles and amyloid plaques, formed during Alzheimer's disease [217, 218]. The six glypicans identified to date are known regulators of BMP/Wnt and Shh signaling pathways [219]. Mechanistically, they elicit their effect through direct binding of specific ligands, including Wnt and Hedgehog proteins, presenting them to cognate receptors. However, glypicans may also serve as (membrane-tethered) ligands in their own right by directly interacting with transmembrane receptors, such as the type-II receptor tyrosine phosphatases (RPTPs) and Leucine-rich repeat transmembrane receptors to modulate RPTP oligomerization and transmembrane signaling [199, 200, 220, 221]. Interestingly, type-II RPTPs influence neuronal morphology and have multiple intracellular binding partners including regulators of Rac/Rho activity [199, 201]. In a neuronal setting, loss of a glypicans (by GDE's) might thus lead to altered RPTP clustering at the plasma membrane with a consequent change in localized levels of tyrosine phosphorylated proteins involved in signaling pathways, like the Rac/Rho balance, that stimulates neurite outgrowth. Interestingly, releasing glypicans from the membrane not only depletes the membrane pool but also generates a soluble protein that may serve a distinctive role by itself. Notably soluble GPC4 and GPC6, secreted by astrocytes, activate synapse formation by recruiting and clustering dendritic AMPA receptors on neighboring membranes [189]. Mechanistically, soluble glypican 4 does so by signaling through presynaptic RPTPδ, leading to the release of presynaptic neuronal pentraxin 1 with consequent AMPA receptor accumulation on the postsynaptic terminal [222]. In line with the previous, mice lacking GPC4 or RPTPs both exhibit defects in synapse formation making them strong candidates for astrocyte-induced synapse homeostasis [189, 223]. Hence, by cleaving glypicans, GDE's could provoke a complex signaling cascade with loss of GPC-RPTP signaling *in cis* while simultaneously activating RPTP signaling *in trans*. Interestingly, GDE3 is highly expressed in GPC4 secreting astrocytes and *in vitro* studies have shown that GDE3 is capable of cleaving GPC4 (data unpublished and unpublished data from Shanthini Sockanathan). Moreover, mice lacking GDE3 exhibit similar synaptic defects as do GPC4-null mice (unpublished data from Shanthini Sockanathan). It is tempting to speculate that GDEs, through glypican cleavage and release, might alter the activation status of one or more transmembrane RPTPs to activate a biphasic neural program.

Candidate ligands

Multiple GPI-anchored ligands play essential roles in the nervous system and although the signaling axis they are involved in are generally well understood, the function of their GPI-anchor is not. The prion protein (PrP) is arguably the most enigmatic example. PrP can be secreted by metalloproteinases or unknown phospholipases [224]. When soluble, the PrP is thought to bind to a receptor for which multiple candidates exist. Interestingly, we have found in *in vitro* studies that PrP is a ligand for GDE2 (unpublished data), potentially being the long sought-after phospholipase for PrP. PrP exists in a normal PrP^{C} or a misfolded version, PrP^{Res}, which is associated with a variety of cognitive disorders like Creutzfeldt-Jakob disease. In contrast to wild type PrP^{C}, when mice express anchorless PrP^{C}, a secreted form is detected that accumulates in plaques, however, a clinical disease never develops [225]. On the contrary, when GPI-PrP and anchorless-PrP expression are combined, it accelerates the clinical symptoms. Based on these observations, the GPI anchor could play a role in the pathogenesis, although the physiological function of anchorless PrP is not well understood.

Ephrin A is another GPI-anchored ligand that is actively secreted from the membrane in glioblastoma cells [226]. Ephrin A belongs to a larger family of ephrins which are ligands for Eph receptor protein-tyrosine kinases. They play an important role during embryonic development and axon growth cone guidance by repelling migrating axons [227]. Ephrin signaling is complex and includes multiple distinct ligands and receptors. In general, when membrane bound, ephrin A ligands bind to their cognate receptor on opposing cells to mediate cell-cell communication that signals in both directions [228]. However, when cleaved, ephrin A is still able bind and activate its receptor, leading to, among others things, growth cone collapse [226]. Why ephrin A is secreted and whether phospholipases are involved is unknown.

Neurotrophic receptors

A GPI-anchored receptor specifically expressed in neurons is the ciliary neurotrophic factor receptor A (CNTFRa). CNTFRa is a member of the alpha-helical cytokine family and plays an important role during brain development [229]. CNTFRa enhances neuronal survival while deletion is embryonic lethal [230]. Upon ligand binding, by CNTF, CNTFRa forms a tripartite complex with LIFRβ and GP130 to activate the downstream signaling pathways JAK/STAT [231]. CNTFRa can be cleaved and soluble CNTFR is measured in cerebrospinal fluid [232]. Intriguingly, cleaved CNTFRa is still able to bind CNTF and LIFRβ to activate signaling pathways in distant cells, although the underlying mechanism is unclear [233, 234].

Another receptor, the Glial cell line-derived neurotrophic factor receptor (GDNFR or GFRα1) is a GPI-anchored receptor for GDNF and neurturin (NTN). GFRα1 is a coreceptor

that forms a complex with the Ret tyrosine kinase and plays key roles in neuron survival and differentiation. In fractionation studies GFRα1 was mostly recovered in the soluble fraction, indicating GFRα1 is actively secreted [235]. Moreover, the soluble form of the receptor is still able to promote neuronal survival in the presence of its ligand (GDNF), suggesting a distinctive role for the cleaved receptor in distant signaling [236].

Adhesion molecules

Contactin1 is an essential neuronal adhesion molecule and mutations in the gene cause a familial form of lethal congenital myopathy [237]. When membrane bound, contactin1 is involved in neurite extension and adhesion [238]. Interestingly though, when added in a soluble form, contactin1 continued to enhance neurite outgrowth without affecting adhesion [239]. When cerebrospinal fluid, a natural source of soluble contactin1, was used similar affects were observed that could be partially blocked by inhibitory antibodies. The underlying mechanism could be binding of contactin1 to PTPRζ which was shown to promote oligodendrocyte maturation [240]. How contactin1 is cleaved and if cleavage is essential for normal development is unknown.

Conclusion

While only a selection of GPI-anchored ligands, receptors and adhesion molecules present in the nervous system are discussed, they are all found in a soluble form. Until recently, little was known about the mechanisms and physiological relevance underlying their shedding. The finding that a cell-intrinsic phosphodiesterase, GDE2/GDPD5, hydrolyzes GPI anchors to modulate signaling pathways and alters cell behavior sheds new light on the mystery of these GPI-anchored proteins [110, 137, 138]. All GDE studies performed so far have focused on loss of function effects after cleavage of a GPI-anchored protein, but recent findings have shown that some soluble GPI-anchored proteins (e.g. GPC4) serve a distinct function by itself [189]. Therefore, the scenario that GDE's could be ligand forming instead of "cleave and release" type enzymes warrants further study. Future studies should also address whether (some of) these proteins are indeed GDE substrates, and how their cleavage and release may impact neuronal physiology. It will also be important to understand how neuronal GDE expression and activity are regulated by either cell-intrinsic or cell-extrinsic cues. Finally, from a clinical perspective, the new findings suggest that activation or inhibition of the GDE signaling pathway by pharmacological means might be of benefit to patients having low or high GDE expression levels. However, since GDE's are not classic phosphodiesterases, it will be quite challenging to develop drug-like allosteric activators or inhibitors.